LUT UNIVERSITY
LUT School of Energy Systems
LUT Mechanical Engineering

Pekka Virtanen

VALIDATION OF ELECTRIC MOTOR'S LAMINATE ROTOR STACK CHARACTERISTICS FOR FINITE ELEMENT MODELLING

31.8.2021

Examiners: Professor Jussi Sopanen
D.Sc. (Tech.) Eerik Sikanen

ABSTRACT

LUT University
LUT School of Energy Systems
LUT Mechanical Engineering

Pekka Virtanen

Validation of electric motor's laminate rotor stack characteristics for finite element modelling

Master's Thesis

2021

72 pages, 30 figures, 14 tables, 11 equations and 1 appendix

Examiners: Prof. Jussi Sopanen
D.Sc. (Tech.) Eerik Sikanen

Keywords: Finite element analysis, electric machine, electric motor, laminate rotor stack, material properties, validation and verification

Green thinking and different environmental regulations have pushed electric motors from the small-scale consumer products to even the main power source of the modern cars. Increasing number of applications mean that the technology is rapidly developed, and the performance of the systems continuously analyzed and optimized.

The goal of this thesis is to study the material properties of electric motor's laminated rotor stack and create as accurate digital model of the motor as possible. Finite element models are created for two different electric motors and numerical modal analysis is performed. The material properties of the laminated rotor stack are validated by comparing the results the numerical modal analysis to experimental measurements. The whole motor assembly is validated to acquire information of the complete system and the behavior of the rotor in it.

The models of both motors were successfully validated with the numerical results being close to the measurements. The results imply that laminated rotor stack does not significantly increase the stiffness of the rotor and the Young's modulus rather matches with various polymers and fiberboard.

TIIVISTELMÄ

LUT-Yliopisto
LUT School of Energy Systems
LUT Kone

Pekka Virtanen

Sähkömoottorin laminoidun levypakan ominaisuuksien validointi elementtimallinnusta varten

Diplomityö

2021

72 sivua, 30 kuvaa, 14 taulukkoa, 11 yhtälöä ja 1 liite

Tarkastajat: Professori Jussi Sopanen
Tutkijatohtori Eerik Sikanen

Hakusanat: Elementti menetelmä, sähkökoneet, sähkömoottorit, laminoitu roottoripakka, materiaaliominaisuudet, validointi ja verifikaatio

Vihreä ajattelu ja erilaiset ympäristöön liittyvät määräykset ovat ajaneet sähkömoottorit pienen mittakaavan kuluttajalaitteista jopa nykyautojen päävoimanlähteeksi. Lisääntyneet käyttökohteet lisäävät myös teknologian kehitystahtia ja laitteiden suorituskyvyn jatkuvaa analysointia ja optimointia.

Tämän diplomityön tavoitteena on tutkia sähkömoottorien laminoidun roottoripakan materiaaliominaisuuksia ja luoda moottorista mahdollisimman tarkka digitaalinen malli. Tutkimus tehdään kahdelle erilaiselle sähkömoottorille luomalla laitteista digitaaliset mallit elementtimenetelmää hyödyntäen ja suorittamalla numeerinen moodianalyysi. Roottoripakan materiaaliominaisuudet validoidaan vertaamalla moodianalyysin tuloksia kokeellisiin mittauksiin. Myös koko moottori malli validoidaan, jotta saadaan kerättyä dataa roottorista mahdollisimman realistisissa olosuhteissa.

Validointiprosessi onnistui molempien moottorien kanssa. Kerätyt tulokset viittaavat, että roottoripakka ei oikeastaan lisää roottorin jäykkyyttä. Roottoripakan kimmomoduuli vastaa nimittäin polymeerejä ja kuitulevyä.

ACKNOWLEDGEMENTS

This thesis was successfully completed with the help of several counterparts. I would like to thank them all for the help and support during my thesis work.

Special thanks to my supervisors Prof. Jussi Sopanen and D.Sc. (Tech.) Eerik Sikanen from LUT University, for the support and guidance you have given during my final studies. I would also like to thank the laboratory of machine dynamics for performing the experimental measurements.

Thank you, Danfoss Editron Lappeenranta, for the opportunity and interesting thesis topic. Thank you Mikko Piispanen, Marko Tuuha and Anssi Suuronen for supervising my thesis work.

Pekka Virtanen
August 2021
Lappeenranta, Finland

TABLE OF CONTENTS

LIST OF SYMBOLS AND ABBREVIATIONS

SYMBOLS

A_d	Un-Threaded Area of the Bolt
A_t	Bolt's tensile Area
$\boldsymbol{a}$	Eigen Vector
$\mathbf{C}$	Damping Matrix
D_{bolt}	Bolt Head Diameter
d_{bolt}	Bolt Diameter
E_{CORE}	Young's Modulus of the Cylinder
E_{Cu}	Young's Modulus of Copper Windings
$\boldsymbol{F}$	Force Vector
h	Thickness
I_D	Inertia Value of the Metal Sheets
$\mathbf{K}$	Stiffness Matrix
K_C	Core Spring Coefficient
k_{cu}	Cross section of the Conductor to the Total Area of Slot
l_t	Thread Length
l_d	Un-Threaded Length
l_{eff}	Effective Grip Length
$\mathbf{M}$	Mass Matrix
M_D	Mass Value of the Metal Sheet
n	Iteration Step
p_t	Increase in the Shaft Diameter
$\boldsymbol{u}$	Displacement Vector
$\dot{\boldsymbol{u}}$	Velocity Vector
$\ddot{\boldsymbol{u}}$	Acceleration Vector

ρ_{cu}	Density of Copper
ρ_{eq}	Equivalent Mass Density
ρ_{ins}	Density of Insulation
ϕ_E	Diameter of the Rotor Shaft
ϕ_{EQV}	Equivalent Diameter of the Rotor Shaft
ω	Eigen Value

ABBREVIATIONS

AC	Alternative Current
DE	Drive End
DOF	Degrees of Freedom
EM1	Electric Machine 1
EM2	Electric Machine 2
EMA	Experimental Modal Analysis
FE	Finite Element
FEA	Finite Element Analysis
FEM	Finite Element Method
LDV	Laser Doppler Vibrometer
NDE	Non-Drive End
PM	Permanent Magnet
R&D	Research and Development
SRPM	Synchronous Reluctance Assisted Permanent Magnet
V&V	Verification and Validation

1 INTRODUCTION

Electric motors have been used in different everyday products like refrigerators, washing machines and electric fans for a long time already, but due to the environmental regulations set around the world, the technology has been rapidly utilized also in other industries. Electric drivetrains are now used also in modern cars, heavy machinery, and marine applications.

Common electric motor types in industry are alternative current (AC) induction motors and permanent magnet (PM) motors. Each of these motors naturally has their own advantages and disadvantages with overlapping functionalities, but are simple, brushless, and easily maintained. (Murphy 2012; Hanejko 2020.). These two electric motor types are structurally very similar, and their main components are frame, stator, rotor, bearings, and end bells (Figure 1).

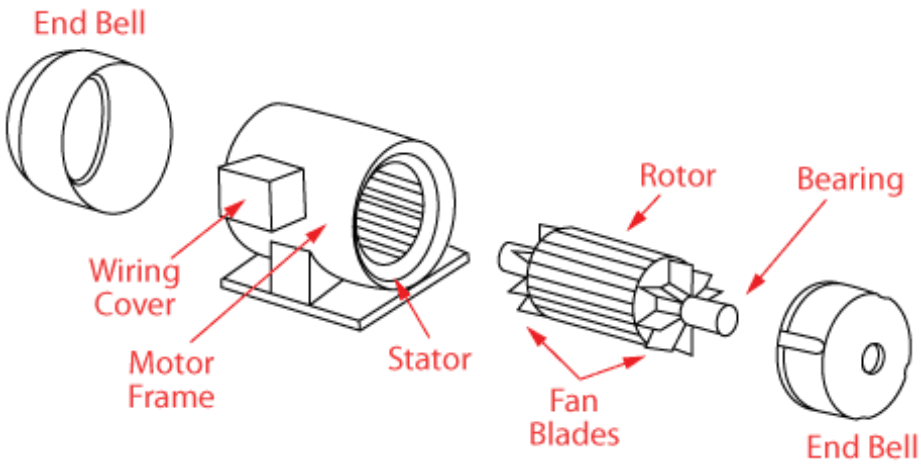

Figure 1. The main structure of induction motors (Hanejko 2020).

AC Induction motors, also referred as asynchronous motors, have a stationary stator with rotating magnetic field, and a rotor with a cage structure called “squirrel cage”. The induced current creates a magnetic field that is attracted by the stator field and creates rotation to the rotor. PM motors have also stationary stator with a rotating magnetic field like induction motors, but uses permanent magnets in the rotor (Figure 2). These magnets are attracted by the magnetic field of the stator and create rotation.

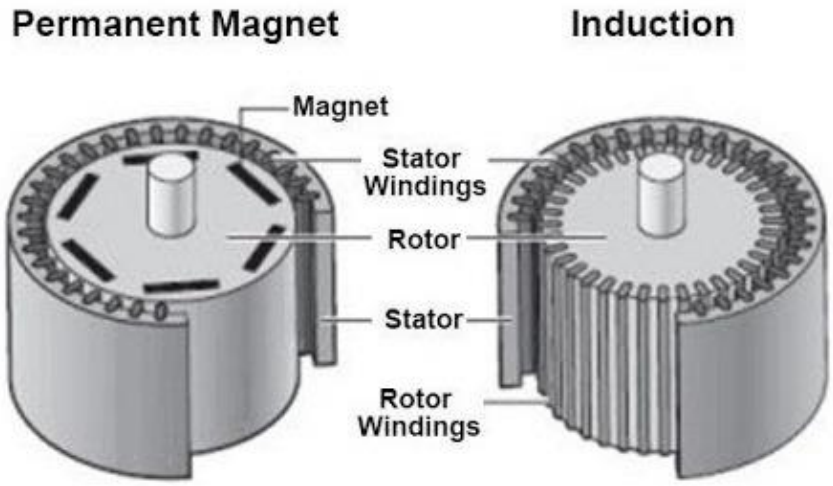

Figure 2. The structure of permanent magnet motors VS induction motor (Hanejko 2020).

This master's thesis work is done with Danfoss Editron Oy and LUT University. Danfoss Editron offers electric drivetrain systems for marine, off-highway and on-highway industries. Danfoss Editron designs, manufactures, and delivers a range of electric motors utilizing permanent magnets. (Danfoss 2021.)

1.1 Research background

Like in any designing process, the products are nowadays first studied in digital form. This can be done in various ways, one of which is finite element analysis (FEA). These digital analyses are used to estimate the performance of the product in various situations even before the first prototypes are made. This makes it possible to save some development costs and helps to present the product's performance to the customers interested in buying them before manufacturing it.

Usually, while creating finite element (FE) models, some parameters and structures can be estimated to prevent too complex models and/or to decrease the computing load. These estimations can be done by using various simplifying formulas or by modifying the 3D models of the product. These estimations, however, always create some error to the results and the significance to them needs to be evaluated.

1.2 Research problem

FE modelling gives approximate solutions according to the user inputs. The validity of these analyses can be verified with experimental modal analysis (EMA). After EMA, it is sometimes noticed that these measurements do not give results that correspond the simulations well enough. Usually, the reason is found from the FE models. The differences between the two can usually be explained with incorrect modelling of the structure, improper boundary conditions and assumptions of the parameters or model order errors. (Cavalini 2015, p. 1; Mottershead 1993, p. 347.)

In PM and induction motor applications, there is a rotor stack which consists of several thin metal plates that are compressed together. In PM motors this rotor stack also includes the permanent magnets (Figure 3).

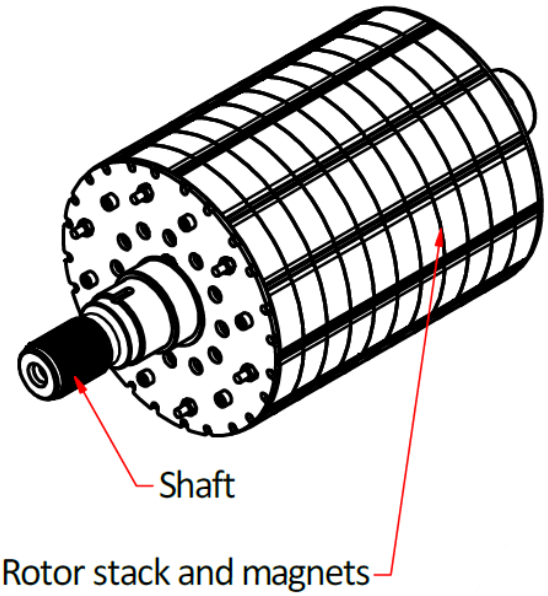

Figure 3. The rotor of permanent magnet motor is covered with rotor stack and magnets.

This plate stack would be demanding to model accurately so the structure is usually simplified. However as mentioned previously, these estimations can cause error to the results and lead to the need of re-determining some material properties.

1.3 Goals

The goal of this research is to create FE models of Danfoss' electric motors and find the most accurate parameters for the plate stack. This is done by comparing the vibration analysis of the model to the vibration measurements for the real motor and tuning the material parameters in the FE model.

1.3.1 Research question

This research is meant to answer the following questions:

- How to simplify the electric motor models for FEA purposes?
- How is the experimental modal analysis performed to measure the critical frequencies of electric motors and their components?
- How to find the vibration modes of electric motor and its components?
- How to validate FE models with experimental methods?
- How much the validated numerical analysis differs from the results of experimental modal analysis?

1.3.2 Hypothesis

Similar studies have been made for various systems, where the authors have successfully matched the first modes of the system with the experimental results. Including LUT University has experience from vibration measurements and model validation. By utilizing similar principles and the results collected from previously made studies, it should be possible to validate the generated models.

1.4 Research methods

During this study, several research methods are applied. First, the literature review is done to examine the possible ways to create the FE models, how to perform the vibration measurements for the electric motor and how to perform model validation. The second part of this study includes the practical part. This study includes the modelling and vibration analysis of the electric motor by using finite element method (FEM) and the vibration measurements performed to the real motor. The FE models and vibration analysis is done using FE software called Ansys. The vibration measurements are done with equipment from LUT University. Lastly the vibration measurements are used to validate the generated FE models.

1.5 Framing

This thesis studies electric machines of Danfoss Editron (Danfoss), which utilize synchronous reluctance assisted permanent magnet (SRPM) technology. Danfoss has a large range of motors and this paper concentrates on two models particularly. These motors are called electric machine 1 (EM1) and electric machine 2 (EM2). The first, EM1, belongs to the smaller end of Danfoss' line, weighing 300 kg, and the second motor, EM2, is from the larger end, weighting over 1 000 kg. There are some design differences between the smaller and larger motors, and by selecting two motors from different size groups it is possible to collect data for both size groups. (Danfoss 2021.)

For the simulations, the models are assumed as perfect examples with no defects or damage. However, the motors used for the measurements, are for research and development (R&D) and have been used for several cycles in various test setups.

The vibration measurements require proper equipment to achieve reliable and valid test results. All the used equipment is provided by LUT University and the laboratory of machine dynamics. The usable measurement methods are limited by the available equipment.

1.6 Contribution of the thesis

With electric motors or any rotating machines, the dynamic properties are important to know especially close to the working speeds. Experimental modal analysis and simulated dynamic models make it possible to find these properties and even optimize the structure of the machine.

By following this work Danfoss, or any company in that matter, can collect valuable information of how accurate their current dynamic models are and how they can be perfected. Especially in the applications where laminated structures are used.

2 THEORY OF MODAL ANALYSIS AND MODEL VALIDATION

This chapter introduces the general theory for FEM, natural frequencies, vibration measurements and model updating, but also takes a closer look to few details in the scope of this study like laminated rotor stack and the supporting bearings.

2.1 Finite element method

FEM is a numerical method used to solve the response of complicated structures, that would be difficult to solve analytically. In this method, the analyzed structure is divided into smaller parts, elements, which together create a mesh on studied structure (Figure 4).

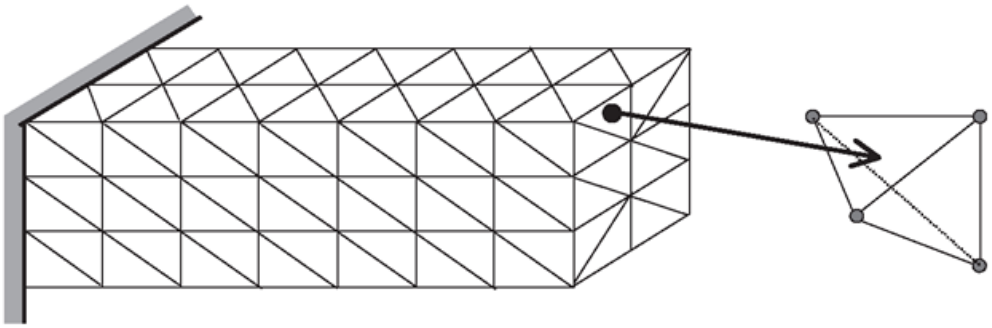

Figure 4. Three-dimensional structure meshed with solid elements (what-when-how).

In three-dimensional structures, like shown in figure 4, elements have 3 translational and 3 rotational degrees of freedom (DOF) along *X*, *Y* and *Z*-axes. So, in total each element has 6 DOFs. If the structure was only in two dimensions, the amount of DOFs would decrease to 4.

In FEM, one can use several kinds of element types and probably the most common ones are beam, plate and solid elements. Some parts of structures can be simplified into beam and plate elements to make the meshing and computing easier, but usually solids are still needed for complex geometries (Skotny 2019).

Elements usually consist of two main shapes: triangles and squares. With these shapes, one can create 2 or 3 dimensional elements (Figure 5).

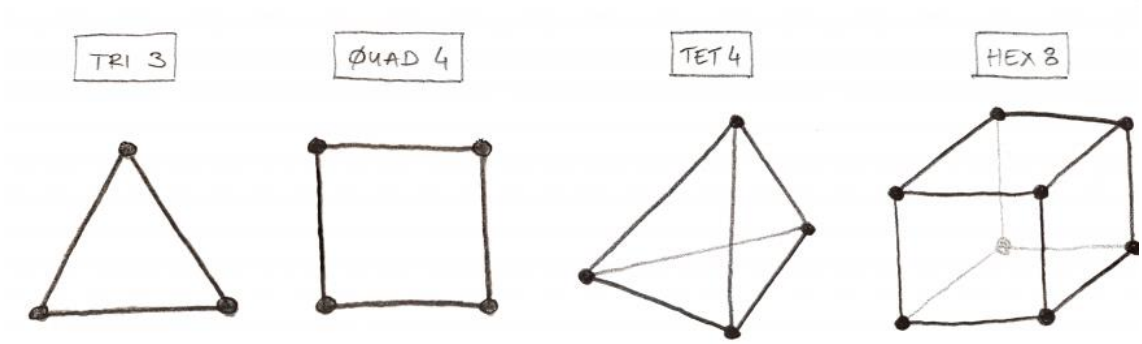

Figure 5. Different element shapes for 2D and 3D elements (Skotny 2019).

The tetrahedron, TET4, and hexahedron, HEX8, element types presented in figure 5, are used in 3D structures. According to Skotny (2019) the triangular elements are usually not so as good as quadratic for FEM. This is because the number of elements needed is high, and they can behave too rigidly. By using hexahedral elements, these problems can be reduced. However, tetrahedrons are still used in more complex features and details of the structure. (Skotny 2019.)

The accuracy of the model can be increased by increasing the number of element connection points, called nodes. One way is to increase the number of elements by reducing the elements size. Another way without increasing the number of elements is to use quadratic elements (Figure 6).

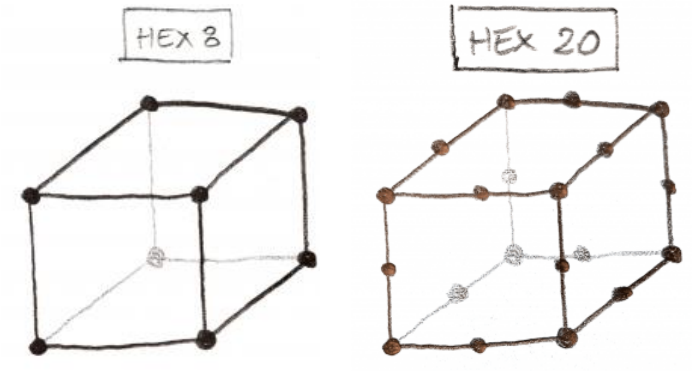

Figure 6. HEX8 and HEX20 solid 3D elements (Skotny 2019).

As seen from the HEX8 and HEX20 elements in figure 6, quadratic elements have node points on the corners but also in the middle of the element. This adds additional solution points to the model without the increase in number of elements.

The sufficient number of nodes is always dependent of the application. The more nodes there are the more detailed mesh will be but with a cost in the computing time. In comparison to shell and plate elements, with solid elements the number of nodes is greatly increased since elements cover the whole component also through their thickness and not only on the surface. According to Skotny, it is not favorable to use one solid element across the thickness of any component and shell or beam elements should be used instead. (Skotny 2019.)

Each node contains an equation of motion. By transforming the elements from their local coordinate system to the structures global coordinate system and solving the equation of motion of each node, an approximated model can be created (Nutakor 2014, p. 16). In FEM based software like Ansys, the equation of motion (EOM) of a system with *n* degrees of freedom, can be presented with equation:

$$\mathbf{M}\ddot{\boldsymbol{u}} + \mathbf{C}\dot{\boldsymbol{u}} + \mathbf{K}\boldsymbol{u} = \boldsymbol{F} \tag{1}$$

Here (Equation 1) $\mathbf{M}$ is $n \times n$ mass matrix, $\mathbf{C}$ is $n \times n$ damping matrix and $\mathbf{K}$ is $n \times n$ stiffness matrix. Vectors $\boldsymbol{u}$, $\dot{\boldsymbol{u}}$ and $\ddot{\boldsymbol{u}}$ represent the systems deformation and its derivatives while $\boldsymbol{F}$ represents the external forces affecting the system. When studying undamped free natural frequencies of the system, the damping matrix, $\mathbf{C}$, and the force vector $\boldsymbol{F}$ can be set to zero. With these assumptions the EOM for undamped and unforced system can be simplified. (Čorović & Miljavec 2020, Pp. 2-3; Nutakor 2014, Pp. 13-14.)

$$\mathbf{M}\ddot{\boldsymbol{u}} + \mathbf{K}\boldsymbol{u} = 0 \tag{2}$$

With equation of motion like presented in equation 2, the FEM software can solve the eigenvalues and eigen vectors of the system. Eigenvalues are the natural frequencies of the system, where the system oscillates without external force. These frequencies are associated with eigenvectors, mode shapes, that represent the relative displacement of the system masses to the nodes. Eigen values, ω, and eigen vector, $\boldsymbol{a}$, can be solved from equation:

$$(\mathbf{K} - \omega_i{}^2 \cdot \mathbf{M}) \cdot \boldsymbol{a_i} = 0 \tag{3}$$

The number of DOFs in the system equals the number of natural frequencies from equation 3. When the system is vibrating according to the systems i^{th} natural frequency, ω_i, the masses displacements follow the corresponding eigenvector $\boldsymbol{a}_i$. (Čorović & Miljavec 2020, p. 3.)

With FEA, it is important to notice the high number of inputs this method requires from the parameters to the tuning of the mesh, and like mentioned previously, improper parameters are one cause of errors in simulated structures (Cavalini 2015, p. 1; Mottershead 1993, p. 347). (Nutakor 2014, p. 16.) It is usually also required that the studied geometries need to be remodeled for the analysis. This is done because of the number of small details that CAD files usually contain, since they are meant for manufacturing purposes. By removing these small details from the system and simplifying design the computation becomes much less demanding. (Skotny 2019.)

2.2 Modelling of the laminated rotor stack

The laminated stack of electric motor consists of several thin metal plates to enhance the performance of the motor. The dynamic properties of the laminated stack are not the same as a solid metal block of the same dimensions, so the structure cannot be estimated in such way and alternative solutions must be found (Garvey et al. 2004, p. 193; Čepon, Pirnat & Boltežar 2012, p. 3153).

For the modelling of the laminated structures, Santos, Luersen and Bavastri (2013), reviewed three ways to simulate laminated structures utilizing beam elements. These methods are: Equivalent diameter model, branched model and unbranched model. The first of which is most widely used for modelling any part assembled on a shaft. (Santos, Luersen & Bavastri 2013, p. 460.)

In the equivalent diameter model, the diameter of the rotor shaft, ϕ_E, is increased for the area of laminated stack. This value is called ϕ_{EQV}. With the increased diameter, the intention is to simulate the stiffening effect of the laminate stack (Figure 7).

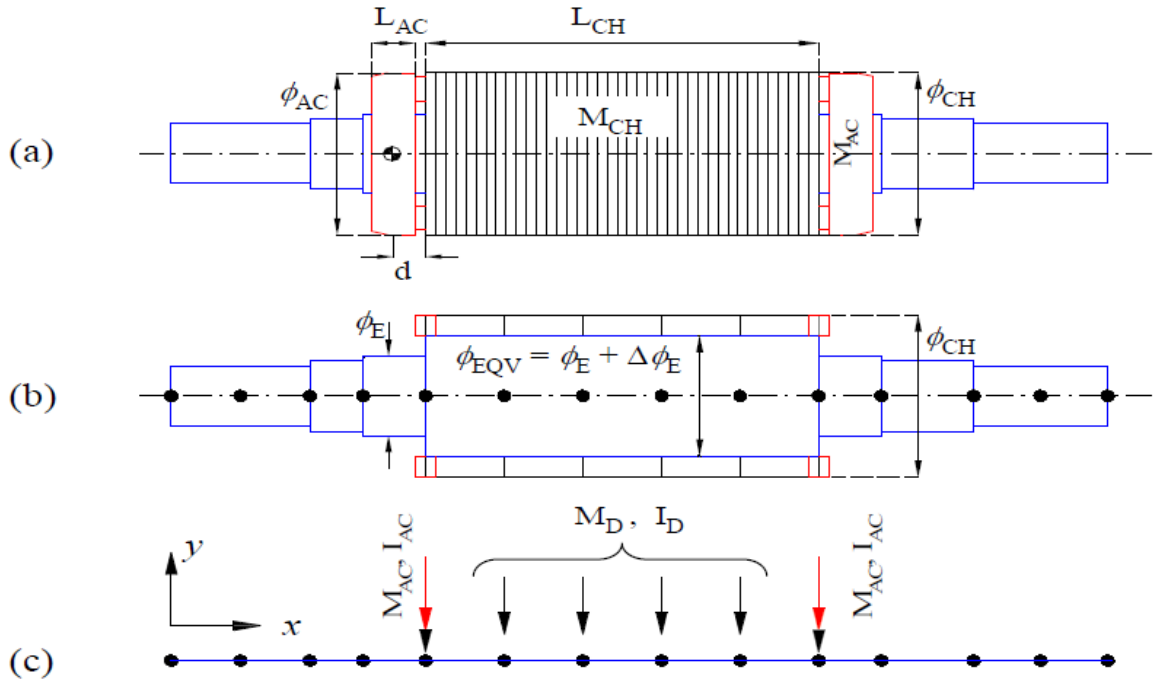

Figure 7. The equivalent diameter method increases the diameter of the rotor shaft and divides the laminate stack mass and inertia values to the shaft nodes (Santos et al. 2013, p. 460).

The mass and inertia values, M_D and I_D, of the metal sheets are divided to the nodes of the shaft (Figure 7). In this method, the only unknown parameter is the increase in the shaft diameter, p_t, which determines the ϕ_{EQV}:

$$\phi_{EQV} = \phi_E \cdot (1 + p_t) \tag{4}$$

According to Santos et al. with this formula (Equation 4) the increase in the shaft diameter, p_t, varies from 0.28 to 0.36. Alternatively, ϕ_{EQV} can also be determined with

$$\phi_{EQV} = \phi_E + (\phi_{CH} - \phi_E) \cdot p_t \tag{5},$$

where ϕ_{CH} is the outer diameter of the laminate stack. With this equation, the value of p_t varies from 0.17 to 0.23. However, with both methods the value of p_t varies from the application and the natural vibration mode shape of the rotor. (Santos et al. 2013, Pp. 460–461.)

Another way to simplify the laminated structure is by using an unbranched model (Santos et al. 2013, p. 461). In this method the laminate stack is modelled as a hollow cylinder on top of the shaft (Figure 8).

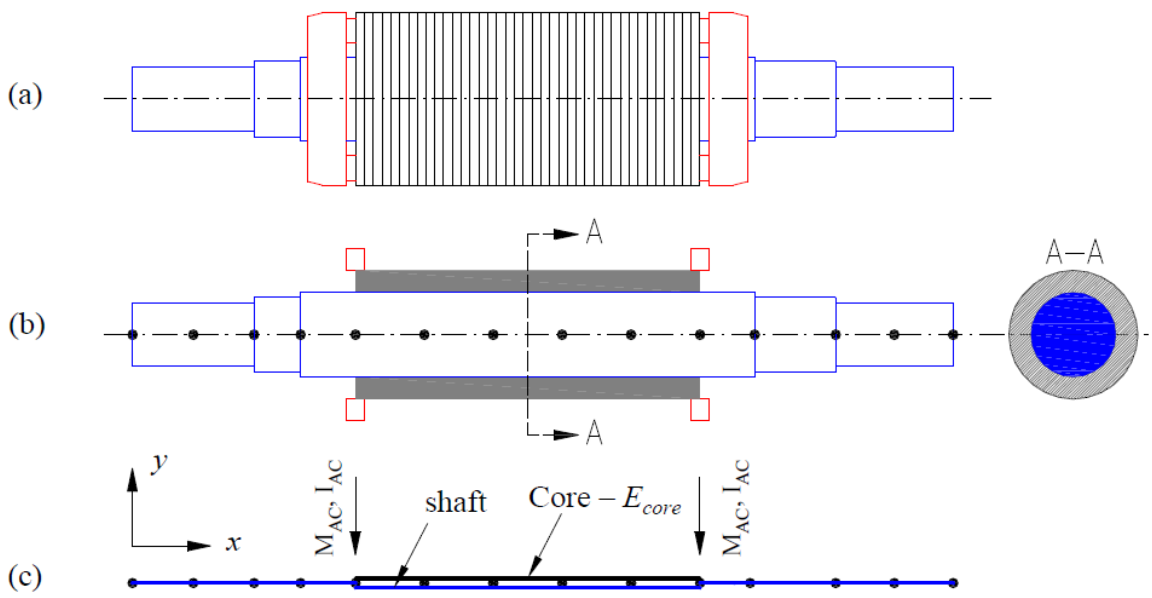

Figure 8. In unbranched model the laminate stack is modelled as hollow cylinder on top of the rotor shaft (Santos et al. 2013, p. 462).

The cylinder and shaft are modelled with two isotropic beam elements. The elastic properties of this cylinder are matched with the laminate stack. For the model, presented by Santos et al., the unknown parameter is the Young's modulus of the cylinder E_{CORE}. (Santos et al. 2013, p. 461.)

Isotropic cylinder, as introduced in the unbranched model, can be modelled to the rotor shaft so that the shaft and the cylinder are connected from node points to each other with spring elements (Figure 9).

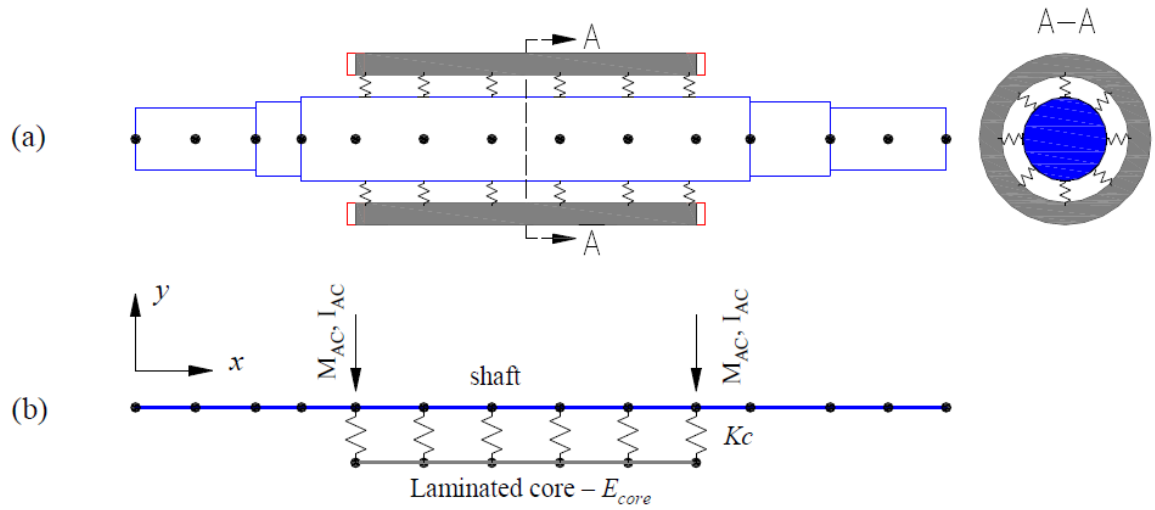

Figure 9. In branched model the laminate stack is modelled as hollow cylinder, which is attached to the rotor shaft with spring elements (Santos et al. 2013, p. 462).

In this model the material properties of the cylinder are matched with the shaft and the spring coefficient K_C is tuned to match the results with the real system. Garvey, Penny, Friswell and Lees (2004) used branched model in similar way but divided the cylinder into rings. These rings have identical mass and inertia properties and are connected elastically to the shaft and the rings right next to them (Garvey et al. 2004, p. 199).

From the previously mentioned methods the branched model is the most appropriate for the analysis of laminated structures (Santos et al. 2013, Pp. 470–471; Garvey et al. 2004, Pp. 200–201). According to a study performed by Garvey et al. (2004), the unbranched method can give sufficient results for the first resonance frequencies, but the structure of the model is wrong for proper analysis (Garvey et al. 2004, p. 197).

Santos et al. collected similar results from their study, where they compared all three of the previously mentioned methods. In this comparison the branched model performed clearly the best. The branched model also performed well when tested the robustness of the model. Santos et al. tested how the model performed when calculating the frequencies of multiple rotors with only one parameter value. In this test the average error of the model remained under 5%, which was regarded as a good result. (Santos et al. 2013, Pp. 469–470.)

To take into account the frictional forces between each layer of lamina, Čepon et al. (2012) developed a method to account this in a general laminate model. In this method each layer is modeled, and the tangential and normal direction forces between them estimated with numerical methods. This study was done for a general laminate stack design and thus was possible to maintain the computational efficiency. However, this means that utilizing this method in the dynamical analysis of whole laminate stack, would probably be computationally too demanding. (Čepon et al. 2012, Pp. 3153, 3164.)

Previously mentioned studies utilized more simple beam elements, but another possibility is to use solids. Čorović and Miljavec (2020) studied the modal behavior of interior permanent motor (IPM) with numerical and analytical methods and used experimental measurements to validate the collected results. This study utilized solid elements in the FEA and studied the IPM assembly in multiple cases, which are presented in figure 10.

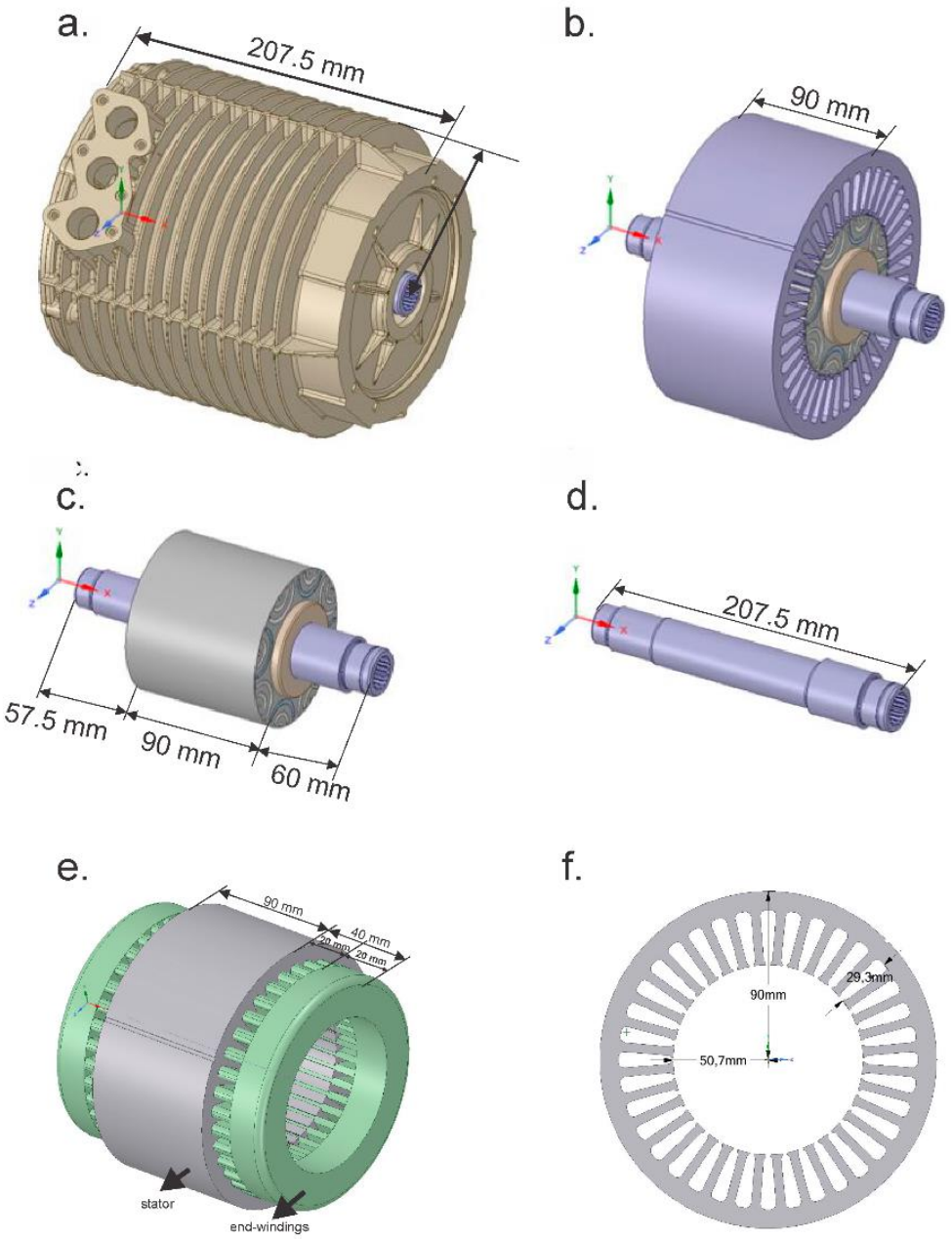

Figure 10. The IPM assembly was studied as a complete assembly (a), assembly without the housing (b), the rotor assembly (c), the shaft only (d), stator and stator windings (e) and stator only (f) (Čorović & Miljavec 2020, p. 4).

Čorović and Miljavec models included all the main components of IPM motors: the housing, stator, slot and end windings, rotor stack and the rotor shaft. The paper also included studies about the response of the rotor stack with and without the permanent magnets, the stator with and without the windings and the effect of the bearings to the system. (Čorović & Miljavec 2020, Pp. 3-4.)

According to Čorović and Miljavec, the included permanent magnets have a noticeable effect to the behavior of the rotor stack. Study also noted that studying the dynamic behavior of the rotor, can be utilized to assess the condition of the magnets. As the magnets wear out and become more fragile, new natural frequencies may occur, or the current ones change. (Čorović & Miljavec 2020, p. 22.)

They also noted that including the windings to the stator decreases the natural frequencies of the stator assembly. Čorović and Miljavec used a simplified model for the stator windings, where the equivalent Young's modulus E and mass density ρ_{eq} of the stator windings are estimated with equations:

$$E(k_{cu}) = 0.0004 \cdot {k_{cu}}^2 + 0.0212 \cdot k_{cu} + 0.694 \quad (6)$$

$$\rho_{eq}(k_{cu}) = \rho_{cu} \cdot k_{cu} + \rho_{ins} \cdot (1 - k_{cu}) \quad (7)$$

In equations 6 and 7, k_{cu} represents percentual value for the actual cross-section of the conductor to the total area of the slot and ρ_{cu} and ρ_{ins} represent the mass densities of copper and insulation which the windings are consisting of. This simplification made it possible to model the windings as a solid composite material in FEA with and reach faster computation times. (Čorović & Miljavec 2020, Pp. 5, 22.)

By studying the complete IPM assembly and the assembly without the housing, Čorović and Miljavec were able to show that the housing has an increasing effect to the natural frequencies (Čorović & Miljavec 2020, p. 22). The study of focusing on the stator also noted that some mode shapes might be hidden under other components (Figure 11).

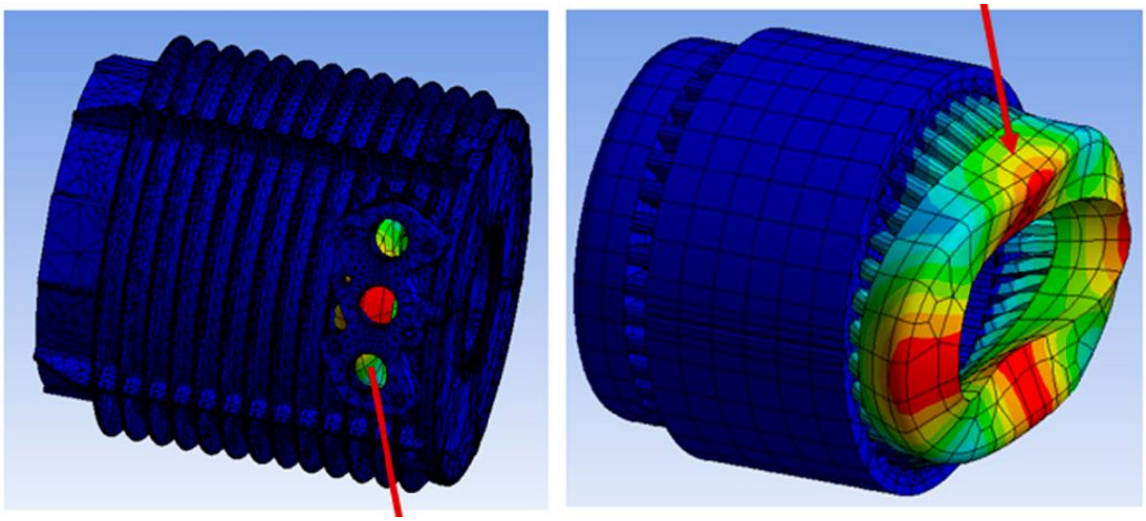

Figure 11. Deformation of the stator windings is not necessarily detected from outside the motor housing (Čorović and Miljavec 2020, p. 15).

As seen from figure 11, it is possible that only the stator is excited without affecting the frame. In this situation the frame of the motor hides the mode shapes of the stator. By hiding the frame from the model, the mode shapes of the stator can be studied easier. (Čorović and Miljavec 2020, p. 15.)

2.3 Modelling of the bearings

Nonlinear factors like the behavior of bearings, can be difficult with finite element methods (Mottershead 1993, p. 347). Kastinen (2019) studied the stiffness values of rolling-element bearings with analytical, numerical, and experimental methods. Kastinen concluded that the results of the experimental methods were 62–85% lower compared to the numerical methods. For numerical analysis, Kastinen used Matlab RoBeDyn toolbox and BearinX software. With BearingX been more accurate of the two. (Kastinen 2019, Pp. 57, 62.)

Analytical methods can also be used to collect rough estimates or starting values while being computationally undemanding (Matyja 2015, Pp. 101–102). In the study performed by Kastinen, analytical methods where even closer to the results of experimental tests than the numerical methods (Kastinen 2019, p. 62). However, these analytical methods are usually rough estimates where the main goal is to decrease the computational time, the results are not necessarily reliable. The study performed by Matyja concluded that the developed

method was able to determine the critical speeds but suffered with low accuracy in critical states (Matyja 2015, p. 101).

2.4 Vibration analysis of an electric motor

Vibration measurements are measurements where the oscillating system is analyzed with different sensors and tools. This oscillation can also be caused manually to have more controlled response. In general, to measure vibrations from the test object, the measurements require excitation, to excite the test object, transducer, to convert the motion of the test subject to electrical signal, and analyzer to process the signal. (Nutakor 2014, Pp. 31–32.)

The excitation can be created with shakers or impact hammers (Figure 12). With shakers one can excite the structure according to the se input signal, but with impact hammer one can excite all the vibration modes at the same time (Nutakor 2014, Pp. 31–32). To increase the repeatability and accuracy of testing, automated impact hammers can be used. These automated systems remove issues like multiple hits or inconsistent force input, which can occur when using manual systems (Alta solutions 2012; Nutakor 2014, p. 32).

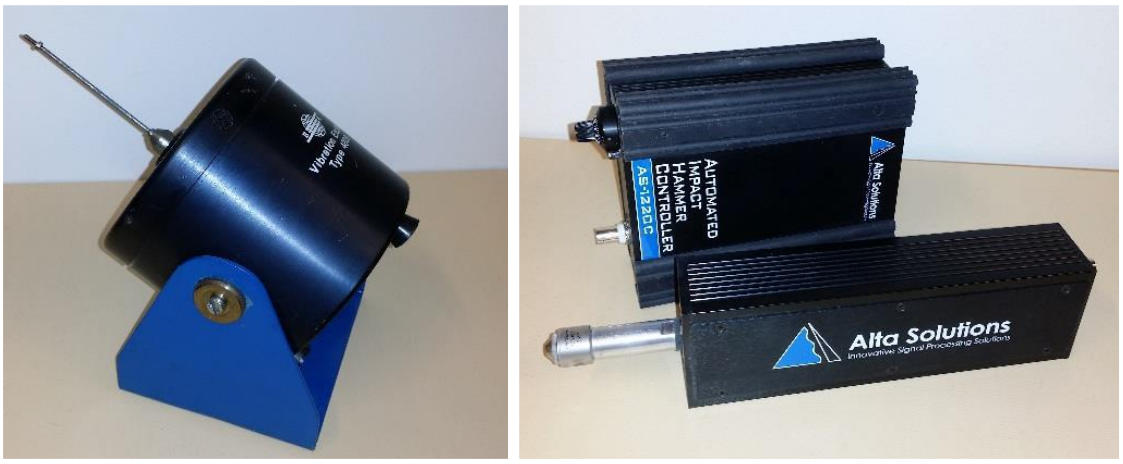

(a) (b)

Figure 12. Excitation can be caused with shakers (a) or impact hammers (b) (Nutakor 2014, p. 32).

According to Devesoft (2021), shakers are usually best option for larger structures. This is because larger structures might need multiple excitation points to excite the structure and using multiple synchronized shakers is easier than using multiple impact hammers. Shakers

also make it possible to do more detailed analysis because it is possible to excite the structure for longer period of time in a specific vibration range. (Devesoft 2021.)

The vibrations of the excited structure can be converted to electrical signal with different sensors. One of which is laser doppler vibrometer (LDV). In comparison for sensors that are physically attached to the test structure, LDV is entirely contact free without any sensors or wires going to the measured structure by using laser in the scanning head (Figure 13).

Figure 13. LDV scanner head from Polytech (Polytec 2021b).

With this method there is no extra mass added to distort the results. In addition, optical measurement method is not affected by temperature changes or loud environment. (Polytec 2021a.)

The basic working principle of the LDV method is presented in figure 14.

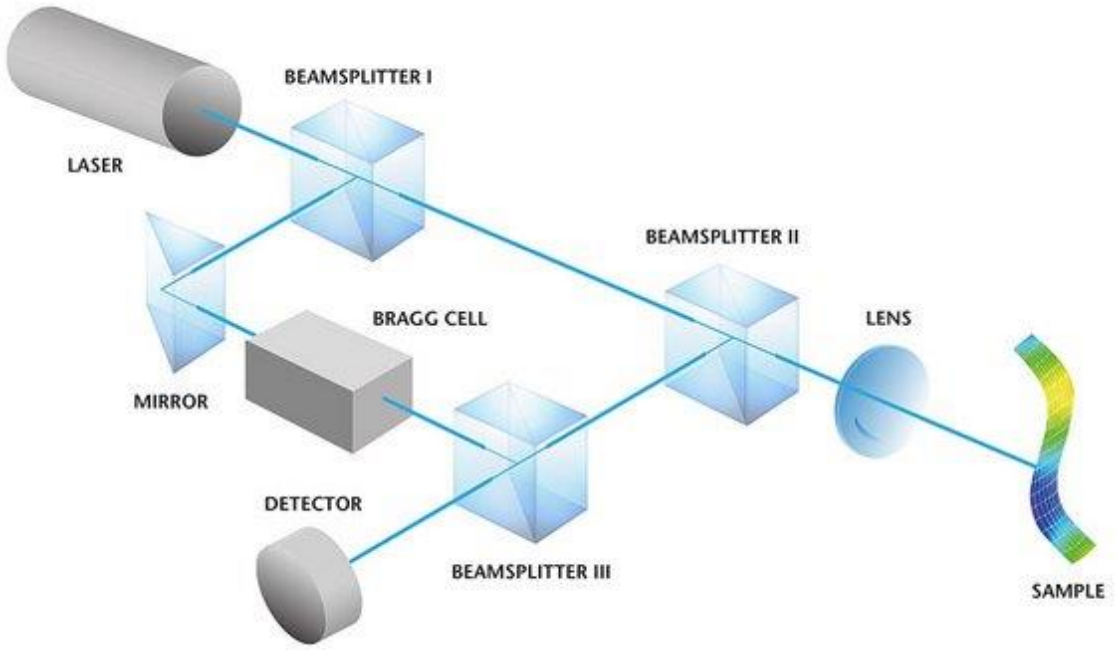

Figure 14. The working principle of LDV system (Polytec 2021a).

As seen from figure 14, the laser coming from the scanning head (Figure 13) is split with a beam splitter so that one beam, called reference beam, goes straight to a detector and the other beam continues to the measured sample. The vibrating surface of the measured sample sends the laser beam back with a different frequency and is also directed to the detector. By comparing the reference signal and the signal coming from the sample, it is possible to find the vibration velocities and displacements of the sample (Polytec 2012.)

Measurements always contain some noise which can distort the collected results. The effect of this noise can be reduced by performing averaging. Averaging is a method where multiple measurements are taken at the same DOF location, and these are averaged. The more averages are chosen the more the noise is reduced from the results. According to Dewesoft, in impact hammer testing 4–8 averages is a good amount. (Dewesoft 2021.)

2.5 Model verification and validation

Model verification and validation (V&V) are important elements of FEA. The verification and validation represent two different things and are situated in different parts of the following flowchart (figure 15).

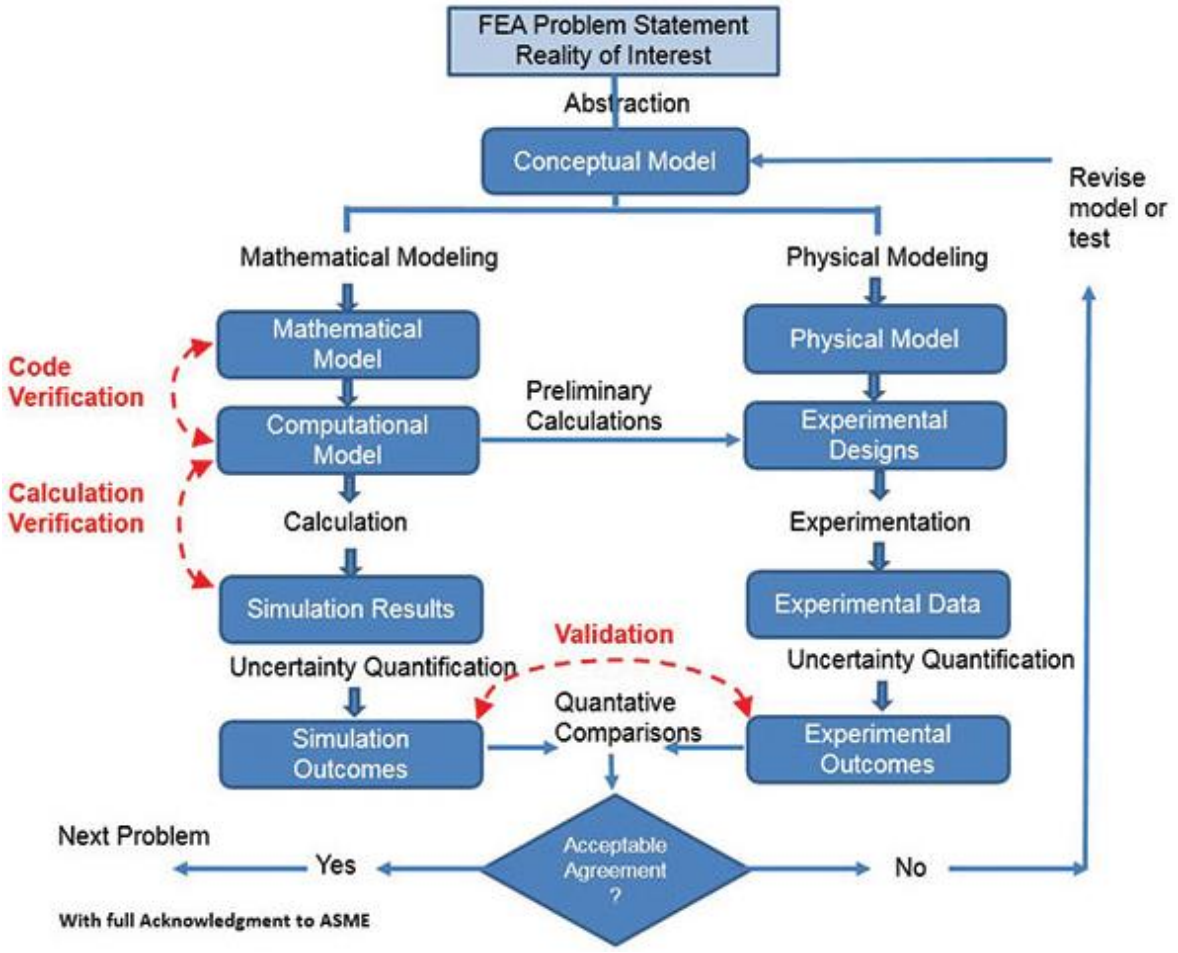

Figure 15. The flowchart for FEA model verification and validation (Abbey 2015).

As seen from the flowchart (figure 15), the V&V can be utilized in different phases of FEA, and product development in general. With model verification purpose is to see if the model functions as intended by comparing the results of the code and simulations to the equations and other reference material. With model validation, the purpose is to see if the results collected from the numeric simulations agree with the results collected from the experimental tests or EMA. (Abbey 2015; Veikos 2016.)

Not only can the EMA be utilized in model validation during the product development phase but also while analyzing the structure during its lifespan. Overtime the structures characteristics may change and the simulations are not valid anymore and need to be updated or the structure maintained.

By utilizing the V&V model, presented in figure 15, the product development process is divided into smaller steps. This does not only help with spotting mistakes but also creates back trackable data and creates a better understanding of the studied system. This way there is better chance of predicting the behavior of the system or finding a mistake that would otherwise cause unnecessary extra work or lead the project in the wrong direction. It is important to remember that in FEA, the models are always approximations of the real systems. Also, the large amount of input parameters makes the method vulnerable for mistakes. Model verification is used to minimize this in the early stages of the process. (Abbey 2015; Veikos 2016.)

3 FE MODELLING OF STUDIED STRUCTURES

In this chapter, the studied structure, the used materials, and constraints used in the FEA are introduced. Original motors are remodeled with Solidworks 2019, and the dynamic analysis is performed with a FEM based software, Ansys 2019R3. The Dynamic analysis is performed for three different cases: The rotor assembly (Case 1), The housing with drive end (DE) plate, non-drive end (NDE) plate and stator with windings (Case 2), and the complete motor assembly (Case 3). The models are analyzed in free-free-conditions, so the model is not constrained in any way, there are no external forces, and the damping of the system is neglected.

Even though the literature suggests modelling the rotor as “branched model”, where the connection between the rotor stack and shaft is modelled with springs, an “unbranched model” is used instead. This is done to concentrate on the material properties of the rotor stack itself. With an unbranched model the connection between the rotor stack and shaft is determined as a bonded contact and the only unknown is stiffness of the rotor stack.

3.1 Structure under research

The studied motors utilize permanent magnet technology. These motors have the similar main components as in the study from Čorović and Miljavec (2020). The main components are presented in table 1.

Table 1. The main components and materials of the PM motor assemblies.

Name	***EM1 Materials***	***EM2 Materials***
Main Frame	Aluminum	Steel
DE plate	Aluminum	Steel
NDE plate	Aluminum	Steel
Stator	Steel	Steel
Stator windings	Copper	Copper
Shaft	Steel	Steel
Rotor stack	Steel	Steel
Rotor end plate	Steel	Steel

EM1 and EM2 share the same materials in all components except in the frame. The main frame of the smaller EM1 is made of aluminum, while EM2's is steel.

The original models, which have been made with the manufacturing in mind, are remodeled and simplified in Solidworks. This is done to remove unnecessary details like small holes and fillets from the geometries to achieve tidier and more accurate mesh during the FE modelling. Using the original CAD files of the motors for the FEA, would also be computationally much more demanding.

3.1.1 Materials

Ansys has in-built CAD software, Space Claim, which is capable to read the part and assembly files from Solidworks. So, bringing the remodeled geometries to Ansys is not a problem. Ansys is not capable of bringing the materials from Solidworks and these are determined from the software's in-built material library (Table 2).

Table 2. Material properties from material library of Ansys.

Motor	***Material***	***Mass Density [kg/m³]***	***Young's Modulus [Pa]***	***Poisson's Ratio***
EM1	Aluminum	2 750	$7 \cdot 10^{10}$	0.33
	Copper	5 500	$1.1 \cdot 10^{11}$	0.34
	Steel	7 700	$2.1 \cdot 10^{11}$	0.33
	EM1 Stack*	7 700	$1.9 \cdot 10^{11}$	0.3
EM2	Steel	7 850	$2.1 \cdot 10^{11}$	0.33
	Copper	5 500	$5 \cdot 10^{8}$	0.34
	EM2 Stack*	7 295	$1.9 \cdot 10^{11}$	0.3

*These materials are modelled as orthotropic.

These material parameters are used for the original models, but the purpose is to update the material properties of both rotor stacks according to the experimental measurements. The material densities are altered so that the masses of the assemblies match their real versions. The material of the rotor stack is determined as orthotropic. The elastic modulus of the rotor stack is assumed to be lower than solid block of steel in the axial direction, where in other directions it is assumed similar. For now, a starting value of $1.9 \cdot 10^{11}$ Pa is set for both rotor stacks.

The reason for the higher Young's modulus of EM1's windings is because of how the models are made (Figure 16).

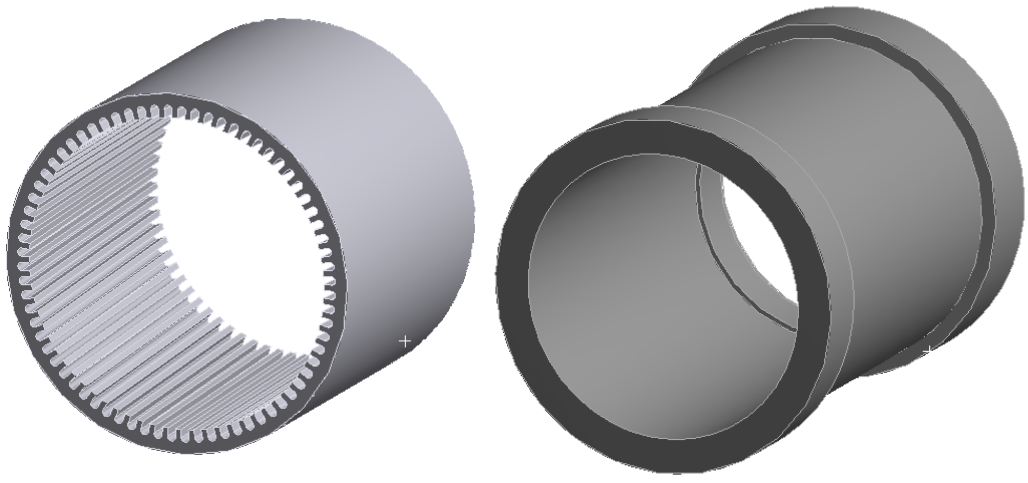

Figure 16. Part of the stator wings are cut off to prevent penetrating geometries.

The windings of EM1 are essentially a solid cylinder with no gaps for the stator wings. The parts of the wings going inside the winding cylinder are cut off to prevent overlapping geometries. For EM2 this is not necessary since the windings have gaps.

3.1.2 Connections

The studied motors contain mainly shrink and bolt connections between the main components. All other connections within the components, like welds, are neglected, and the parts modelled as one block of material. The connections used in FEA between the main components are presented in table 3.

Table 3. Model connection types.

Connection Pair	***Connection Type***
Shaft – Rotor stack	Bonded
Rotor stack – End plates	Bonded
Shaft – DE & NDE plate	Bearing / Spring
Frame – DE & NDE plates	Bonded
Frame – Stator	Bonded

Bonded contacts are used to represent the shrink connections which are located for example between the rotor shaft and laminate stack, and between the motor housing and stator. The endplates of the laminate stack are also connected to the rotor assembly with bonded connections.

The bolt connections between the motor housing and the DE and NDE plates are also modelled with bonded contacts, but with estimated normal stiffness. The stiffness of the bolt itself, K_b, is estimated with equation:

$$K_b = \frac{A_d \cdot A_t \cdot E}{A_d \cdot l_t + A_t \cdot l_d} \tag{8}$$

Here A_t is the tensile area of the bolt and A_d is the un-threaded area of the bolt. Parameters l_t and l_d are the lengths of the threaded and un-threaded portions. (Breunig 2017; Mechanicalc 2021.)

The stiffness of the material clamped between the connection in this tapped joint is estimated with equation:

$$k_m = \frac{\pi \cdot E \cdot d \cdot \tan(30°)}{2 \cdot \ln\left(\frac{l_{eff} \cdot \tan(30°) + D_{bolt} - d_{bolt}) \cdot (D_{bolt} + d_{bolt})}{l_{eff} \cdot \tan(30°) + D_{bolt} + d_{bolt}) \cdot (D_{bolt} - d_{bolt})}\right)} \quad (9),$$

where d_{bolt} and D_{bolt} are the bolt and bolt head diameters. Parameter l_{eff} represents the effective grip length of the bolt, which can be estimated with equations 10 and 11.

$$l_{eff} = h + t/2 \quad , t < d \quad (10)$$

$$l_{eff} = h + d/2 \quad , t \geq d \quad (11)$$

In this case, parameter h, represents the thickness of the end plate and t the depth of the threaded hole in the motor frame. Since in this case $t > d_{bolt}$, equation 11 is used. (Budynas & Nisbett 2011, p. 426; Mechanicalc 2021.)

These two stiffnesses from equations 8 and 9, can be thought to be parallel springs and added together. The acquired stiffnesses for the smaller motor are $13 \cdot 10^6$ N/mm for the drive end of the motor and $21 \cdot 10^6$ N/mm for the non-drive end.

The motor's bearings and their pretension springs are modelled with bearing and spring contacts. Both motors have two bearings, which attach the shaft to the DE and NDE plates. The stiffness values are determined with SKF SimPro Quick software (Figure 17).

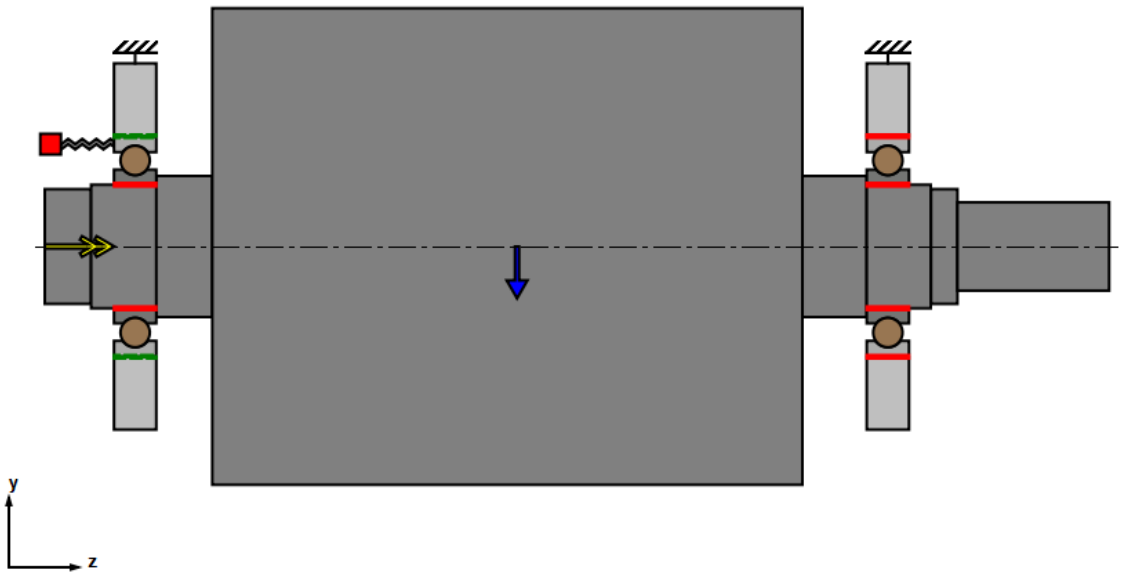

Figure 17. SKF SimPro Quick model of EM1's rotor.

The calculations are made at room temperature, where the rotation speed of the shaft is 1 rpm. The calculations consider the tolerances and lubrication of the system. The stiffness values collected from the SimPro software are presented in table 4.

Table 4. Axial and radial stiffness values of the Bearings collected from SKF SimPro Quick.

Bearing	***Radial Stiffness [N/mm]***	***Axial Stiffness [N/mm]***
EM1 DE	184 333	1 782
EM1 NDE	178 667	1 990
EM2 DE	99 933	1 787
EM2 NDE	143 000	1 577

The values (Table 4) are acquired with the bearing loads and displacements. The pretension springs are added to the axial stiffnesses. The pretension springs are located at the non-drive end of the smaller motor, and at the drive end pf the larger motor.

The bearings are determined between the end plates and the shaft as body-body connection, and the deformation of these connection surfaces are allowed (Figure 18). On default the deformations are not enabled which can cause error to the results.

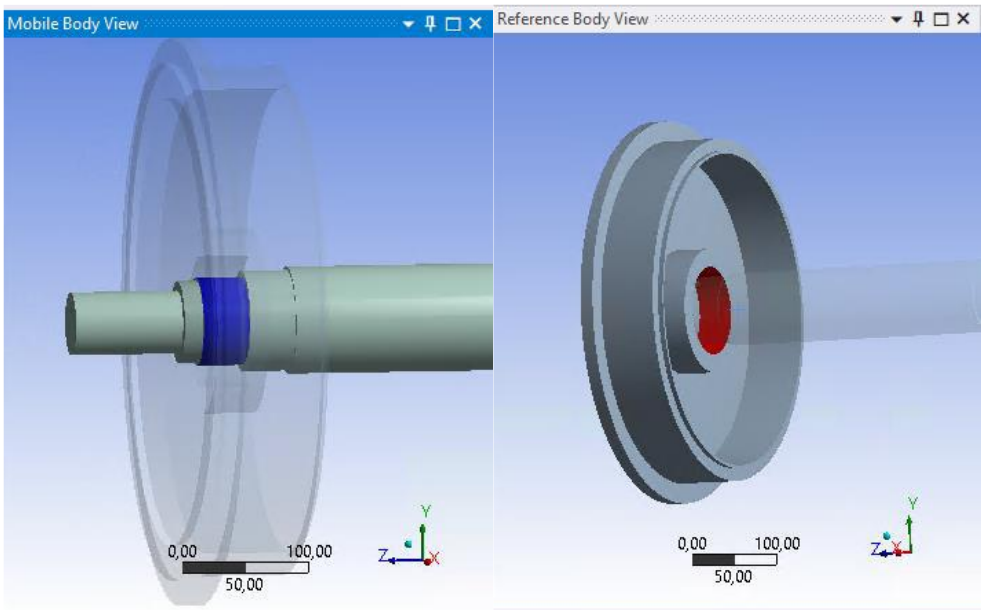

Figure 18. The bearings are set between the shaft and NDE and DE plate (EM1's driving end in the picture).

The radial stiffnesses are set to the bearing connection and they rotate according to the *X* – *Y* plane. The axial stiffnesses are determined by setting a spring between the shaft and end plate and giving it stiffness value along the *Z* – axis.

3.2 Meshing

Ansys automatically generates the mesh for the geometries, which can then be modified with different tools. To achieve a fine and consistent mesh, the sizing and shape of the elements is altered. As mentioned in the literature part of this thesis, HEX8 and HEX20 are usually preferred in the meshing over tetrahedral elements, but in complex areas tetra elements are needed. For this study HEX20 and TET10 elements are used and the created meshes are presented in figure 19.

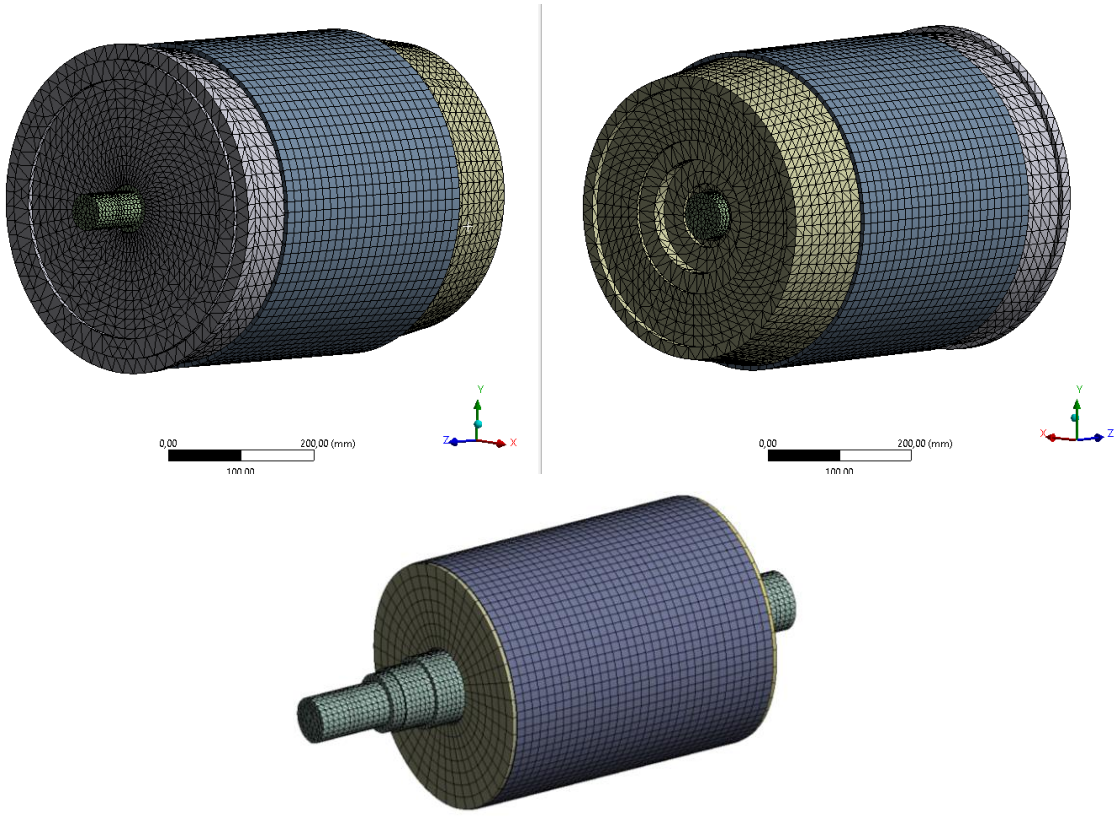

(a)

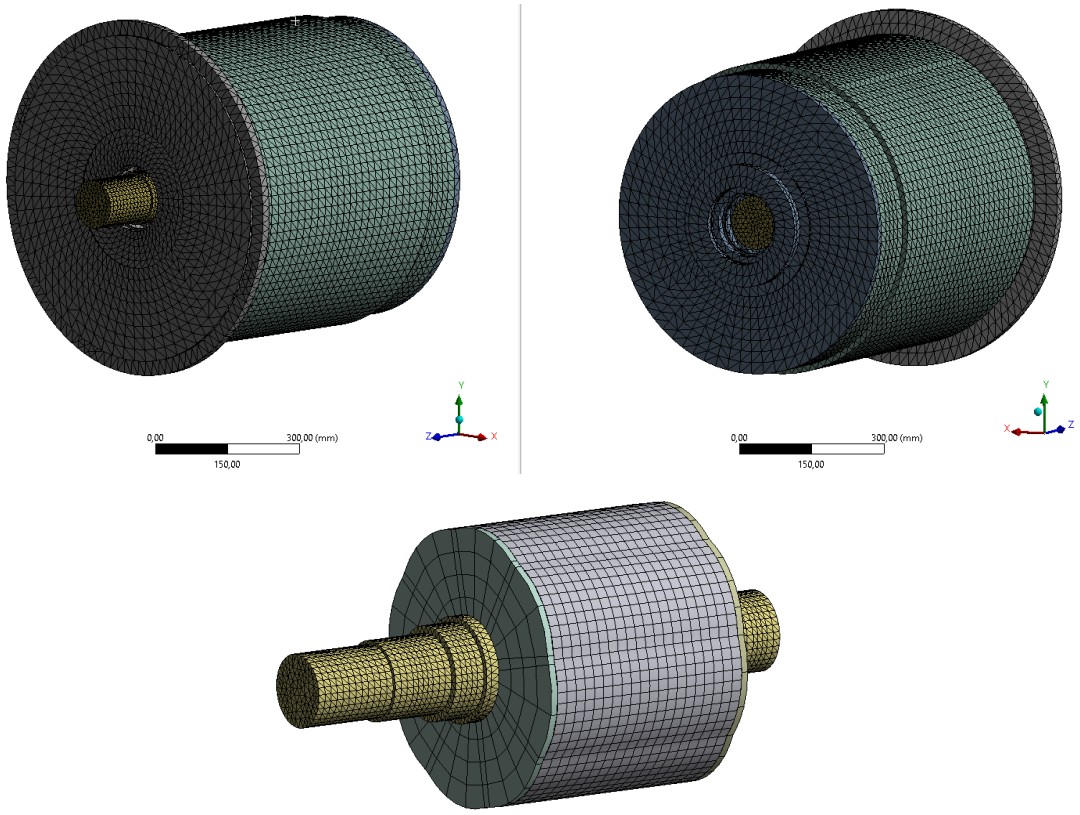

(b)

Figure 19. The mesh for EM1 (a) and the EM2 (b) for FEA.

The mesh of the rotor assembly is presented in figure 19. After the first test runs of modal analysis, it was clear that the largest deformations are occurring e.g., in the rotor shaft and the motor frame. This led to making the mesh finer in these locations. The number of elements in each model are presented in table 5 below.

Table 5. Number of nodes and elements in the finite element models.

Motor	***Case***	***Nodes***	***Elements***
EM1	Case 1 – Rotor	174 315	83 682
	Case 2 – Frame	235 379	67 374
	Case 3 – Motor	319 023	126 219
EM2	Case 1 – Rotor	149 314	82 503
	Case 2 – Frame	411 439	226 681
	Case 3 – Motor	328 125	158 609

The mesh is finest in the areas where the largest and most interesting deformations are expected. In this thesis the areas of interest generally are the rotors. Also, the bearing surfaces are interesting, since the bearing stiffnesses will be validated. Therefore, the end plates and outer shell are also determined with finer mesh. The element sizes are set between 10 – 25 mm with the rotor being the finest and stator and windings being the roughest.

The size difference does not entirely explain the higher number of elements between the frame models between EM1 and EM2. The reason for this difference is also because of the element types. HEX elements were preferred, but were only possible to use in few places. The number of HEX elements is higher in the frame model of EM1, which decreases the number of elements and nodes. To keep the computing time low the density of the mesh is decreased for the full assembly

4 VIBRATION MEASUREMENTS

This chapter introduces the performed vibration measurements for the electric motors. The used equipment and methods, main steps and the overall measurement setup is discussed, and the results are introduced.

4.1 Measuring arrangements

The measurements are performed at Danfoss Editron, by LUT laboratory of machine dynamics. The setup used for this study utilizes laser vibrometer and automated impact hammer to excite the structure and measure the vibrations (Figure 20). For additional information, as reference signal, piezoelectric sensors are used.

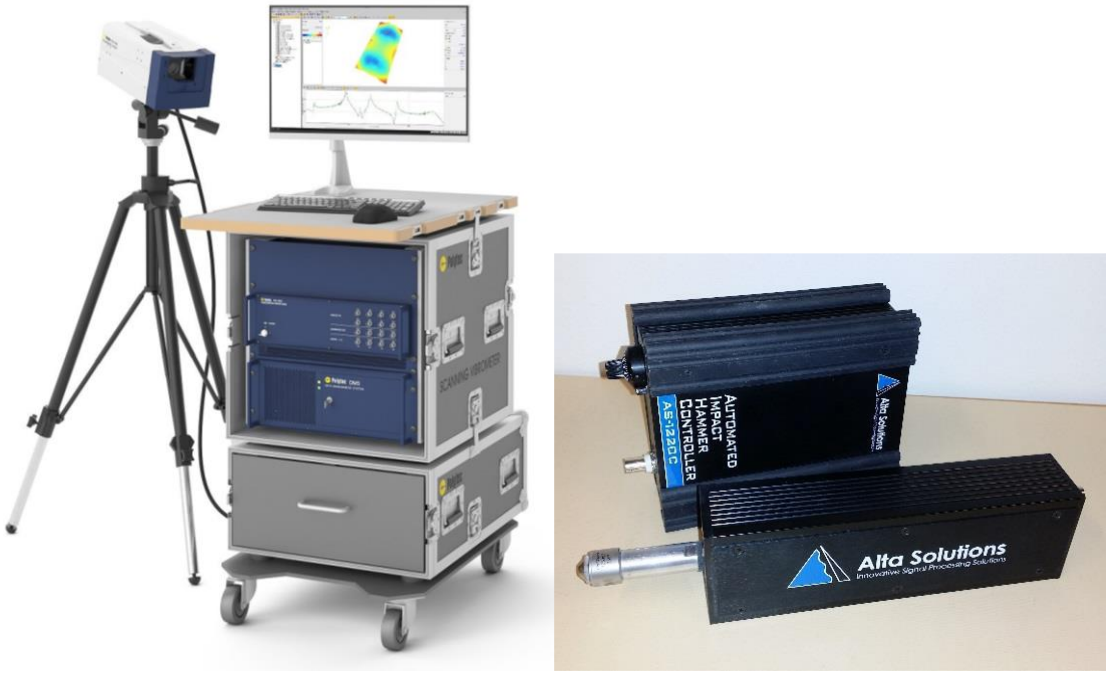

(a) (b)

Figure 20. LDV scanner head (a) and automated impact hammer (b) used in the measurements.

For the measurements, a PSV-500 laser vibrometer (Figure 20a) is used. The impact hammer and its' controller are from Alta solutions (Figure 20b). With this equipment the sample structure is automatically excited with continuous small impacts on the surface.

Testing area is selected so that no large vibrations from running motors, or any other machines, are disturbing the measurements. Testing area also has the required equipment to rotate and move the sample motors between the measurements. The measurement setup is pictured in figure 21.

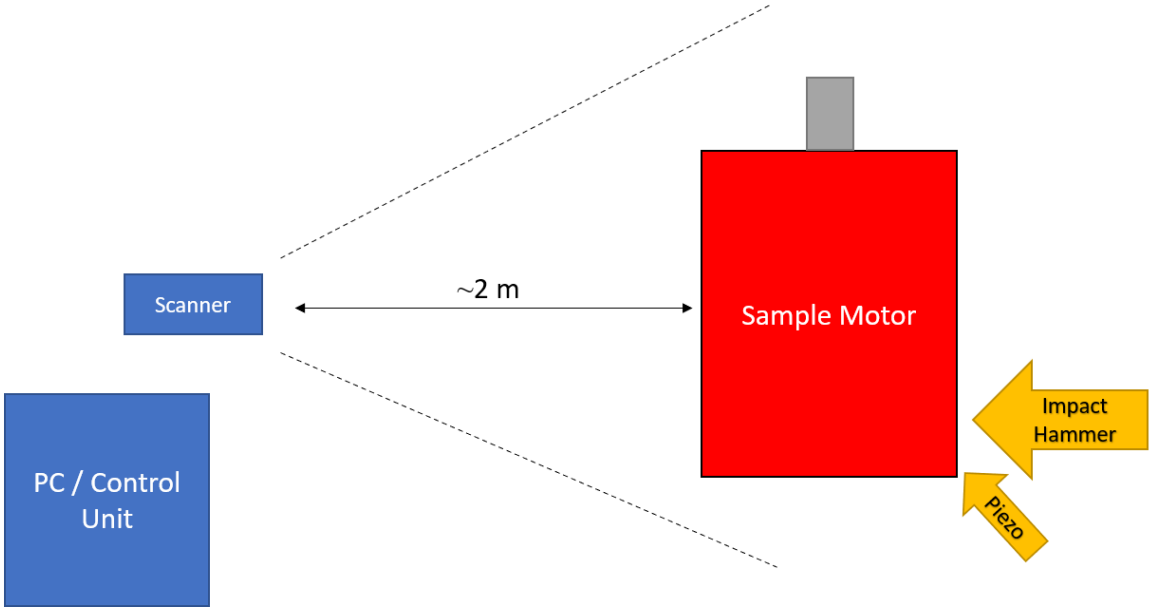

Figure 21. The measurement setup in experimental modal analysis.

The measurements were controlled through the PC and control unit. This control unit includes the controllers and amplifiers required for the equipment used in this experiment.

The scanner head of the laser vibrometer was set to 2 – 3 meters from the sample motors depending on the measured case. With this distance it was possible to get a good image of the sample. Data was successfully collected of the round surface, without the need to rotate the sample.

Impact locations vary for every measurement case and direction, but the impact was generally set to the opposite side of the motor from the scanner head so that the impact is perpendicular to the sample surface and parallel to the laser. For the rotor assembly the excitation was set to the surface of the non-drive end of the shaft. For cases 2 and 3, the excitation was done to the frame. In this setup, piezo sensor was used as a reference signal

to test the generated impact. The piezo sensor was located next to the impact area and connected with a magnet. The aluminum frame of the smaller motor required to add a steel bolt to one of the free bolt holes.

The vibration measurements are performed for three different cases for both two motors: The rotor assembly (Case 1), the housing, end plates and stator (Case 2), and the complete assembly (Case 3). For cases 2 and 3 the measurements are done from 3 directions presented in figure 22.

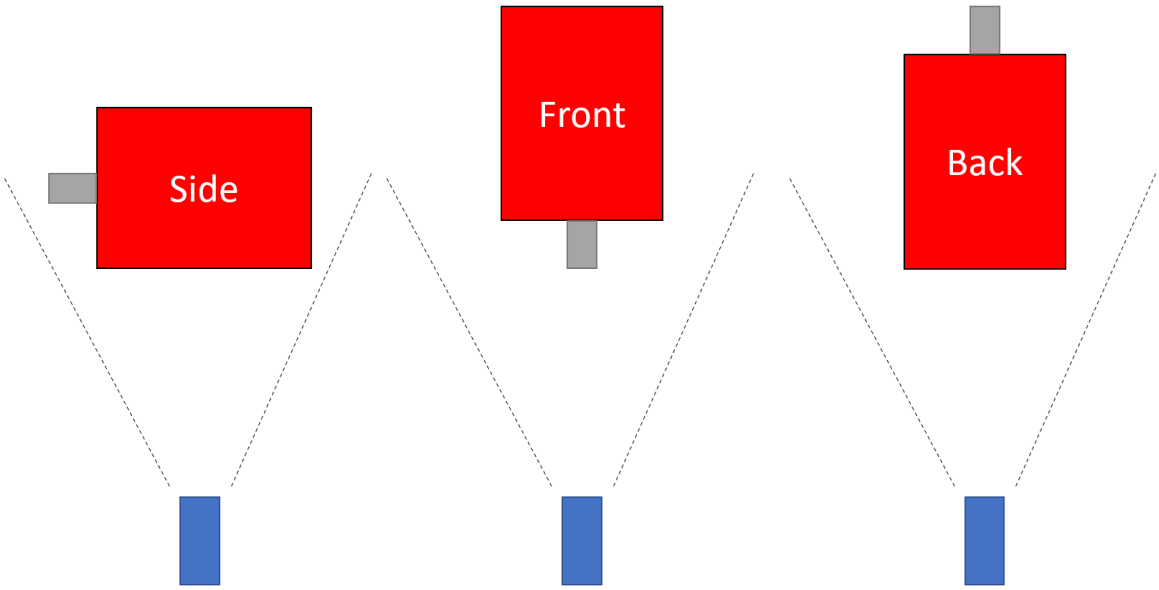

Figure 22. The scanning directions in EMA.

These directions were selected to help recognize the mode shapes of the frame and the end plates with and without the rotor assembly. In addition, the natural frequencies of the bearing supported rotor were determined by scanning drive end of the rotor shaft from the side of (Case 3). The frequencies and modes of the rotor assembly in free-free conditions (Case 1) were measured only from the side, since the most noticeable mode shapes occur towards this plane.

To mimic the free-free conditions of the FEA, all the cases are performed on top of a rubber mat. By using similar support types in both FEA and EMA, the number of variables and distortion in the results can be kept at minimum (Dewesoft 2021).

The initial results are used to help when planning the experimental measurements. According to the initial results, one can see in what range the areas which are interesting to the study, are excited. This helps when selecting the measurement range and resolution, and there will not be a situation where the experimental measurements are not extensive enough or the measurements are made too accurate, which increases the measurement time.

According to the FEA, all the main components are excited at least in one natural frequency in the range of 0 – 4000 Hz. This same range is also set for the experimental measurements. The magnitude of the excitation is measured every 0.3125 seconds for the rotors and every 2.5 seconds for the first motor. For the second motor the magnitude is measured every 1.25 seconds. The meshes of each case can be seen from the EMA results in appendix I.

For the first measurements a higher resolution was used to acquire more accurate natural frequencies. This method used coarser mesh to keep the measurement time short. However, this did not make a noticeable difference to the results, so the rest of the measurements were done using the aforementioned resolution and mesh.

4.2 Results of the vibration measurements

The measurements were successfully completed. Similar mode shapes and frequencies were possible to recognize from the EMA as previously seen in the FEA. This already was promising.

Vibration measurements gave a magnitude-frequency plot (Figure 23) from each individual measurement.

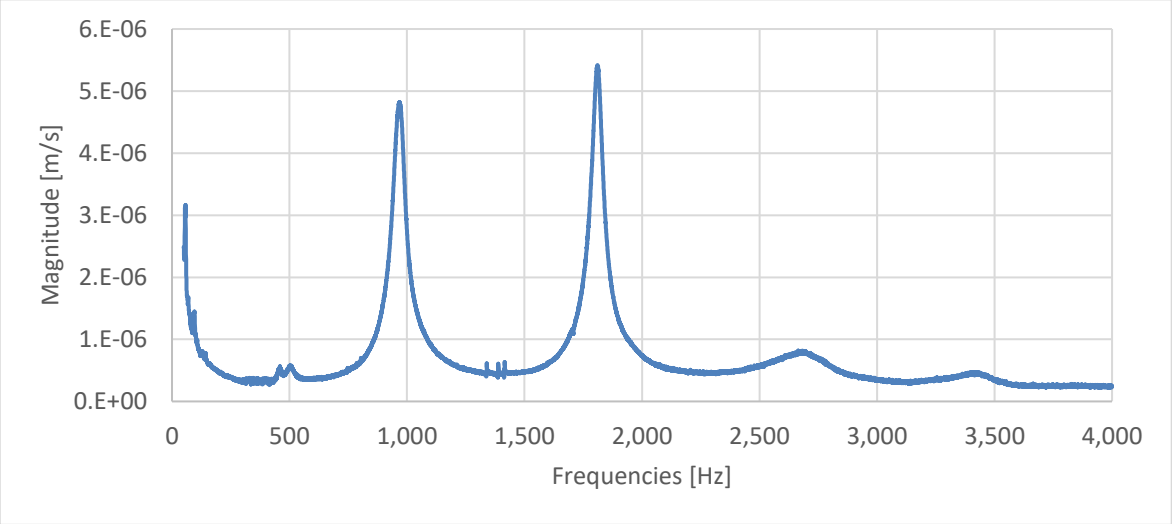

Figure 23. Freq – magnitude plot collected from the measurements of the smaller rotor (Case 1).

These files were taken for post-processing, where the most interesting areas in the graphs were isolated. For modal analysis, these points of interest are the high points in the graph and represent the natural frequencies of the system. In the case presented in figure 23 these points are in approximately 1 000 Hz and 1 750 Hz. The natural frequencies of each case are presented in table 6 below.

Table 6. Natural frequencies (Hz) collected from the EMA for EM1.

No.	***Case 1 - Rotor***	***Case 2 - Frame***	***Case 3 – Motor***
1	968	616	203
2	1811	693	292
3		798	294
4		1000	300
5		1041	339
6		1043	460
7		1144	623
8		1273	726
9		1664	760
10		1970	1160
11		2023	1330
12		2263	1670
13		2294	1700
14		2636	1720
15		2883	1780
16		2923	2230
17		2975	2610
18		3143	2820
19		3330	2850
20		3705	3010

As mentioned before, natural frequencies are associated with mode shapes. After post-processing, these can be inspected with Polytec scan viewer 2.7 software (Figure 24).

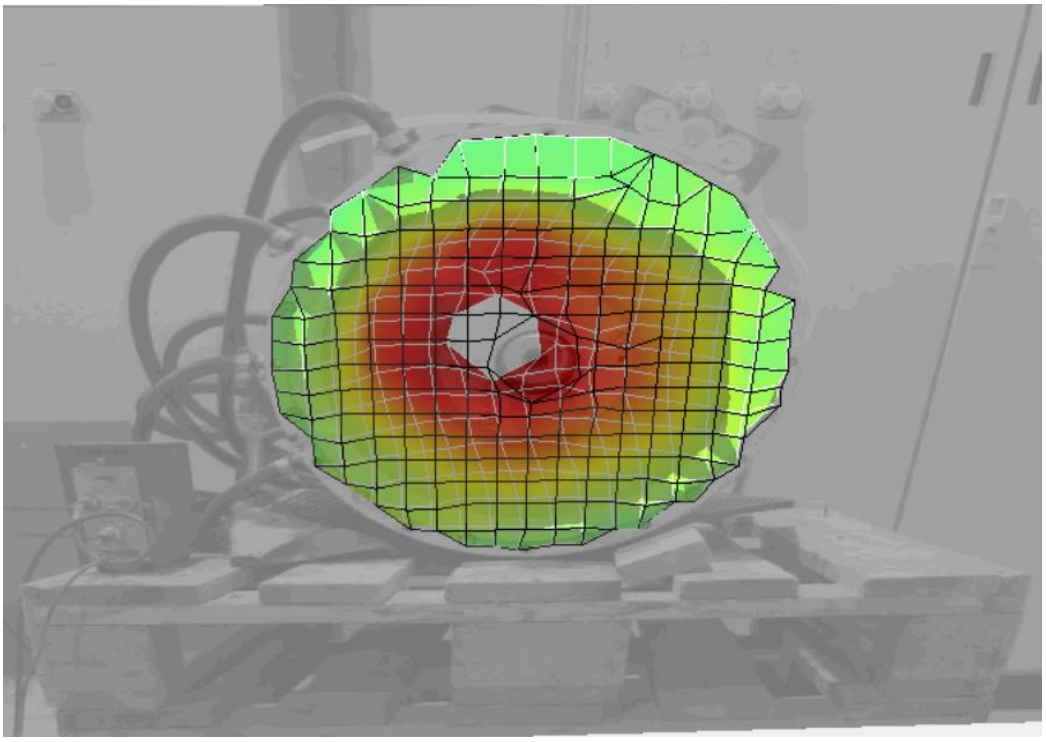

Figure 24. The mode shapes extracted from EMA can be visually inspected.

With the software, it is possible to watch the animation of the meshed surface. The deformations are exaggerated to help the visual analysis. These animations can later be used to recognize the mode shapes and compare them to the initial results from the Ansys dynamic analysis.

5 MODEL UPDATING

This chapter compares the results of the FEA to the practical measurements. The results of the initial FE models are presented first and then the updated ones, along with the explanation of the made modifications. After the validation process the goal is to have models, which present the measured systems as closely as possible an if large differences occur, the reasons are discussed. The validation process itself is similar for both studied motors so the validation process of both are discussed at the same time.

5.1 Comparison of the FE analysis and real-life measurements

To perform the validation, mode shapes from EMA and FEA are selected for comparison. Mode shapes found from EMA should be also found somewhere in the results of the FEA. These similar mode shapes and their natural frequencies are compared to each other.

In EMA the natural frequencies were searched from the range of 0 – 4000 Hz. This means that results outside of that range are not relevant. It is possible that only the first modes between FEA and EMA can be matched as the literature suggested. Therefore, mode shapes of the first natural frequencies are used for the validation process. It is possible that some modes presented in FEA or EMA, are not recognizable in the other or are not even real. This is why selecting only clearly recognizable modes makes the validation process easier.

Since both motors share similar geometry, similar mode shapes can be recognized from them. From the rotors, it is possible to recognize the first and second bending modes. During the first bending mode the rotor bends from the middle like letter “U” or “V”. in the second bending mode the rotor bends like letter “S”.

The common bending vibration modes of the frame's end plates are presented in (figure 25).

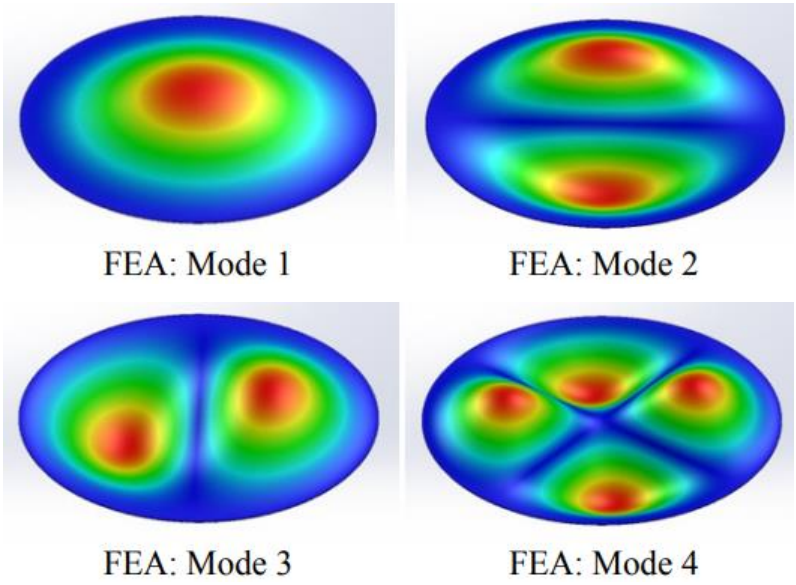

Figure 25. The bending vibration modes of circular plates (Adapted from Tufoi et al. 2014, p. 43).

These mode shapes occur in both modal analyses between the measurements range of 0 – 4 000 Hz. The end plates bend in and out of its plane in 1 – 4 sections. In later modes the number of areas can increase even more. The modes of the midframe also behave in sections that go inwards and outwards, but there are also modes where the frame is bent to a letter "U".

5.2 Improving the FE model parameters

The created FE models contain several approximations in the design itself and the used parameters for the connections and materials. The focus of this thesis is to validate only the material properties of the rotor stack. However, the same principle can be applied and performed for the rest of the models at once. The validation process is done step by step by first validating the rotor and frame models separately and then continuing to the full assembly with the validated sub-assemblies.

5.2.1 Validation of the rotor assembly

From the EMA, only two modes were collected for EM1 and four for EM2. Two shapes from both motors are used for the validation process. For EM1 these are recognized as the

first two bending modes of the system. For EM2, the first recognized mode is the first bending mode. The second mode used for the validation is not a clear 2nd bending mode of the shaft but was found in both EMA and FEA (Figure 26).

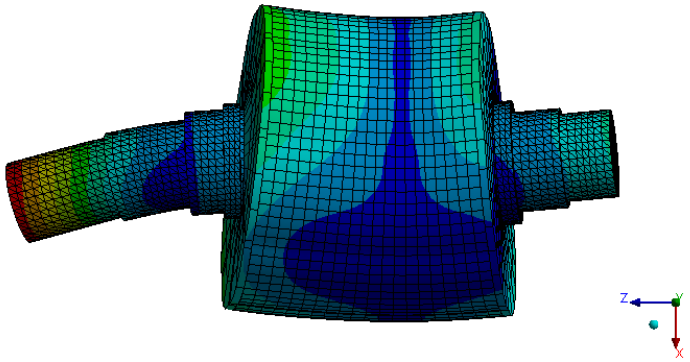

(a)

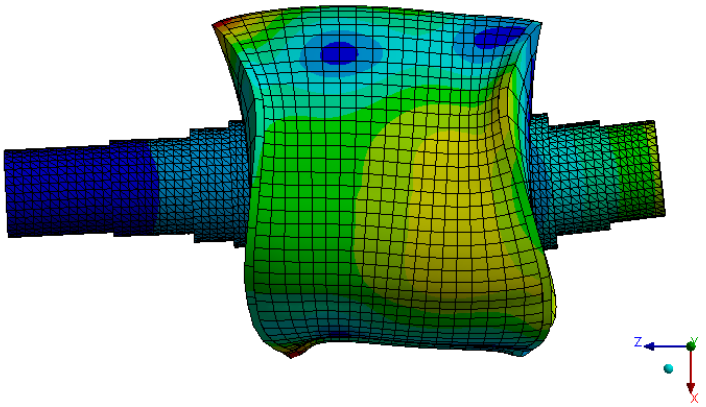

(b)

(c)

Figure 26. A clear second bending mode (a) was found from the FEA, but not from the EMA. For the model validation a mode both found in FEA (b) and EMA (c) was used.

In both FEA and EMA this mode (Figure 26) had a smaller deformation at the drive end of the shaft and larger deformation at the non-drive end. Also, both ends oscillate in opposite directions. These results seem to match and are selected for the validation process. The natural frequencies from FEA are compared to the EMA in table 7.

Table 7. The natural frequencies of the rotors' selected modes before model validation.

Motor	***Mode No.***	***FEA Freqs [Hz]***	***EMA Freqs [Hz]***	***Difference [%]***
EM1	8	1 954	968	102
	10	3 913	1 811	116
EM2	7	1 131	810	40
	9	2 651	1 960	35

The beginning values were acquired with Young's modulus of 190 GPa in axial direction and 210 GPa in radial direction. The results of the smaller rotor have a difference of 100%. The difference in larger rotor is smaller (35 – 40%). Both differences are large, but the starting values for the axial stiffnesses are not yet that far from the values of a normal steel. However, it might be that using the unbranched method makes the models to behave too rigidly. The reason for the larger differences in the EM1's model compared to EM2, might simply be because of the design differences. The larger mass and shaft diameter of the EM2 could make it behave more rigidly already.

To improve the FEA, the axial Young's moduli of the rotor stacks are decreased, as the hypothesis was that the Young's modulus of a rotor stack will be lower than a solid block of steel. By testing descending values, it was found that axial Young's moduli of 4.2 GPa and 2.4 GPa would give the smallest differences to the results of EMA. These results are presented in table 8.

Table 8. The natural frequencies of the rotors after model validation.

Motor	***Mode No.***	***FEA Freqs [Hz]***	***EMA Freqs [Hz]***	***Difference [%]***
EM1	9	969	968	0
	11	1 847	1 811	2
EM2	7	812	810	0
	13	1 945	1 960	-1

As seen from table 8, lowering the Young's modulus changed the order of the modes. This e.g., shifted EM1's 1st and 2nd bending modes from places 8 and 10 to 9 and 11 in the validated model. This was expected since lowering the stiffness of the rotor stack lowers the natural frequencies and therefore moves the related mode shapes. With the updated parameters the difference between FEA and EMA is reduced in both models to < 2%.

5.2.2 Validation of the frame

For the frame, there is no particular point of interest or parameter to validate. The FEA and EMA are still compared to estimate the validity of the frame model. The selected modes for model validation are presented in table below (Table 9).

Table 9. The natural frequencies of the frames' selected modes before model validation.

Motor	***Mode No.***	***Related component***	***FEA Freqs [Hz]***	***EMA Freqs [Hz]***	***Difference [%]***
EM1	7	DE plate	730	799	-8
	8	NDE plate	749	692	8
	9	NDE plate	1 049	1 000	5
	11	DE plate	1 053	1 043	1
	13	Midframe	1 217	1 144	6
	22	Midframe	2 796	2 636	6

Table 9 continues.

Motor	*Mode No.*	*Related component*	*FEA Freqs [Hz]*	*EMA Freqs [Hz]*	*Difference [%]*
EM2	7	NDE plate	485	415	17
	8	DE plate	716	555	30
	9	NDE plate	768	707	7
	11	Midframe	1 052	420	150
	13	DE plate	1 128	1 032	9
	21	Midframe	2 119	1 027	106

These starting values of EM1's FE model are already under 10%. However, the first modes related to DE and NDE plate, where the faces of the plates oscillate in one section, are excited in wrong order and have largest errors. According to the natural frequencies, the DE plate is not stiff enough and the NDE plate is too stiff. However, the next vibration modes (modes 9 and 11 in table 9), which oscillate in two sections, do not have such large differences to EMA. It is possible that the simplification made for the models, have different effect to different mode types.

In the results of EM2, the differences are noticeably larger. Especially mode shapes related to the midframe of the motor, have differences over 100%. The higher difference in the modes that are only related to the midframe, imply that the component could be modelled wrong and behaves too rigidly compared to other components. It was possible to find a natural frequency where both the end plates and the midframe of EM2 are excited at once. In this mode the whole frame is bent into U shape, and the faces of the end plates oscillate in four sections (Figure 27).

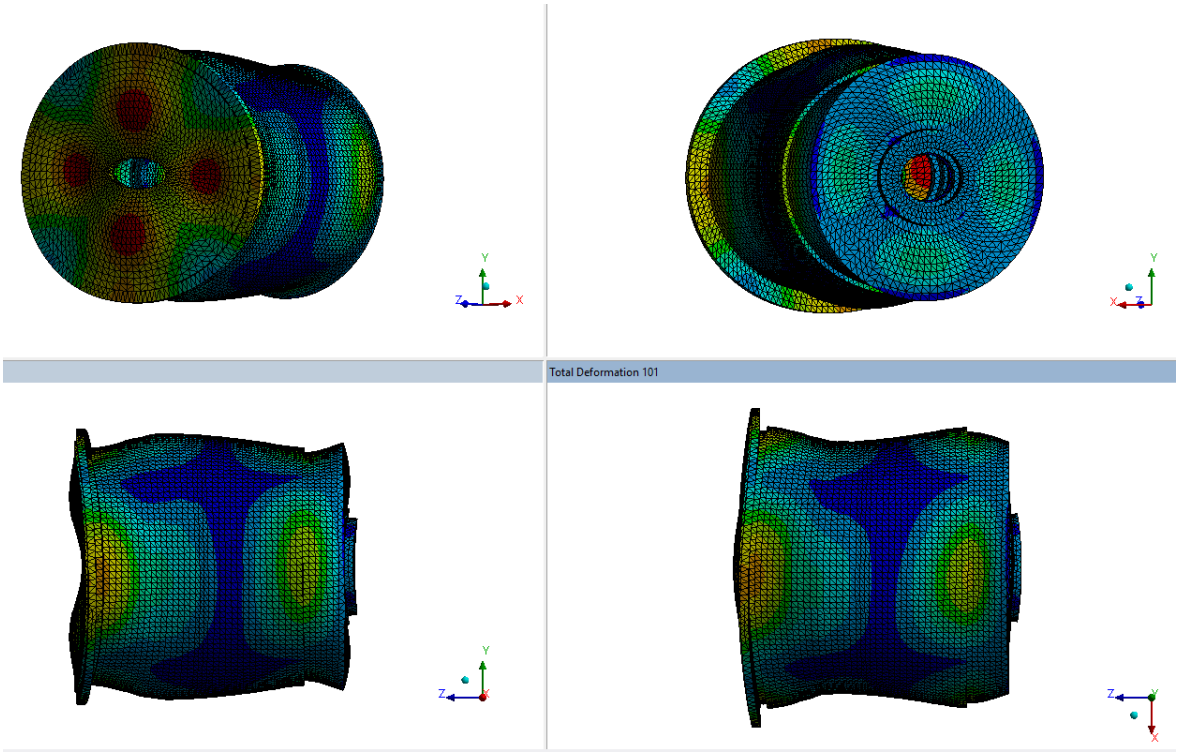

Figure 27. At some natural frequencies, the whole frame structure can be excited at once.

At this frequency, also the end plates have larger errors. This shows that too rigid behavior of the midframe, causes errors also in the natural frequencies of the end plates when the mode shapes are related. Lowering the stiffness of the frame should also reduce the difference regarding the modes related to end plates.

Changing the stiffness values of the bonded connections, which represent the bolt connections between frame and the end plates, had little effect to the results. The bonded contact between the stator and midframe was changed to frictional with friction coefficient of 0.2. This was done to prevent the stator and midframe from behaving too rigidly as one component, when that's not the case in real situation. The material properties were also altered to achieve the results presented in table 10.

Table 10. The natural frequencies of the frames after model validation.

Motor	***Mode No.***	***Related component***	***FEA Freqs [Hz]***	***EMA Freqs [Hz]***	***Difference [%]***
EM1	7	DE plate	730	799	-9
	8	NDE plate	749	692	8
	9	NDE plate	1 048	1 000	5
	11	DE plate	1 052	1 043	1
	13	Midframe	1 170	1 144	2
	22	Midframe	2 660	2 636	1
EM2	N/A	NDE plate	415	415	0
	N/A	Midframe	420	707	0
	N/A	DE plate	527	555	-5
	N/A	NDE plate	679	420	-4
	N/A	DE plate	961	1 032	-7
	N/A	Midframe	1082	1 027	5

The initial models of EM1's frame did not have large differences to the EMA. The most noticeable difference was the behaviors of the end plates in their first vibration modes, where the models were excited in the wrong order when compared to EMA. Changing material properties of the end plates separately was tested, but this also shifted the modes of the plates that were already acceptable. The differences of the mode shapes relating to the midframe of the motor were improved slightly by changing the Young's modulus of the stator from 210 GPa to 170 GPa. Changing the Young's modulus of the stator, had small effect to the endplates of the motor, which were already acceptable.

In the EM2's frame model, the Young's modulus of steel was set to 183 GPa and copper windings to 500 MPa. In the case of stator and midframe, the Young's moduli were decreased even more to 100 GPa. This was done since the modes related to the midframe had significantly higher differences compared to the results of EMA. This for steel structure is a low value and implies that there could be an error in the models. To fix this problem the models need to be redone. However, this thesis is carried through with the current models and the acquired values.

5.2.3 Validation of the full motor assembly

After validating the rotor and the motor frame separately. There should not be need for other adjustments made, except in the connections between these sub-assemblies. In this case they are the bearings which connect the rotor to the frame.

The modes and frequencies of the bearing supported rotor are easy to determine from the FE model. However, in EMA, the rotor is inside the motor and the only visible part of the rotor is the drive end of the shaft. This visible end of the shaft was used to determine the natural frequencies of the rotor, but it is not enough to determine the mode shapes. This means, that finding out which natural frequency corresponds to which mode shape, is not possible and the validation is done just by matching frequencies. However, the modes of the motor frame are as easily recognizable as in the previous case. The selected modes for model validation are presented in table 11.

Table 11. The natural frequencies of the motor's selected modes before model validation.

Motor	***Mode No.***	***Related component***	***FEA Freqs [Hz]***	***EMA Freqs [Hz]***	***Difference [%]***
EM1	N/A	Midframe	232	203	14
	N/A	Rotor	232	292	-21
	N/A	NDE plate	362	294	23
	N/A	Midframe	355	300	18
	N/A	DE plate	388	338	15
	N/A	DE plate	780	726	7
	N/A	NDE plate	795	760	5
	N/A	Rotor	982	1 166	-16
	N/A	Rotor	1948	1 722	13

Table 11 continues.

Motor	***Mode No.***	***Related component***	***FEA Freqs [Hz]***	***EMA Freqs [Hz]***	***Difference [%]***
EM2	N/A	Rotor	155	395	-61
	N/A	NDE plate	426	412	3
	N/A	Midframe	N/A	520	N/A
	N/A	DE plate	627	650	-4
	N/A	NDE plate	699	677	3
	N/A	Midframe	881	935	-6
	N/A	Rotor	844	1020	-17
	N/A	DE plate	991	1020	-3
	N/A	DE plate	1041	1112	-7
	N/A	NDE plate	1041	1117	-7
	N/A	Midframe	1041	1117	-7
	N/A	Rotor	1041	1120	-7

The rotor and frame of both models have already been validated once separately. Overall, the results of the frame seem good. After combining the sub-assemblies into one, the errors might multiply and possibly be the cause of some larger errors. However, the largest differences do come from the modes related to the rotor as assumed.

Literature suggested that bearing stiffnesses estimated with computational methods are usually significantly higher than the ones from experimental measurements (Kastinen 2019, p. 62). However, unlike suggested by literature the initial results suggest that the stiffness of the system needs to be increased. With manual testing of increasing bearing stiffnesses, the following results are collected (Table 12).

Table 12. The natural frequencies of the motor after model validation.

Motor	***Mode No.***	***Related component***	***FEA Freqs [Hz]***	***EMA Freqs [Hz]***	***Difference [%]***
EM1	N/A	Midframe	267	203	32
	N/A	Rotor	267	292	-9
	N/A	NDE plate	267	294	-9
	N/A	Midframe	415	300	38
	N/A	DE plate	288	338	-15
	N/A	DE plate	746	726	3
	N/A	NDE plate	773	760	2
	N/A	Rotor	975	1 166	-16
	N/A	Rotor	1 724	1 722	0
EM2	N/A	Rotor	329	395	-16
	N/A	NDE plate	422	412	2
	N/A	Midframe	560	520	8
	N/A	DE plate	675	650	4
	N/A	NDE plate	791	677	17
	N/A	Midframe	926	935	-1
	N/A	Rotor	976	1020	-4
	N/A	DE plate	976	1020	-4
	N/A	DE plate	1066	1112	-4
	N/A	NDE plate	1066	1117	-5
	N/A	Midframe	1066	1117	-5
	N/A	Rotor	1066	1120	-5

By increasing the radial stiffnesses of the bearings by 170% in the models of EM1 and 900% in the models of EM2, the results presented in table 12 were acquired. These increases resulted in radial stiffnesses of approximately 500 000 N/mm for each end of EM1 and 999 000 – 1 430 000 N/mm for EM2.

After model validation the difference between the EMA and FEA of EM2 are small so the digital model seems to give good approximation of the real system. However, the large differences of the EM1 need to be addressed. The fully assembled motor, which the FE

models were based on, ended up not being ready for the measurements of the fully assembled motor. This forced to use another motor for the measurements. This backup motor was based on the same motor type as EM1 but had been modified with additional cooling system. This cooling system was not entirely removed for the measurements, so the measured and modelled geometries did not match entirely. It is possible that the additional components and possible excess cooling fluid inside could stiffen the system and add mass, which could explain the differences in the results. The full effect of this to the studied system is unknown.

5.3 Summary of the updated materials

After model validation multiple parameters have been updated to achieve as good estimation of the two studied systems as possible. Material properties were only updated for the steel components. The validated properties and their old and new values are presented in table 13 below.

Table 13. The updated Young's moduli values of steel in different components.

	Component	***Original Values [GPa]***	***Updated Values [GPa]***
EM1	*Rotor Stack*	*190*	*4.2*
	Stator	*210*	*170*
EM2	*Rotor Stack*	*190*	*2.4*
	Stator and Frame	*210*	*100*
	DE and NDE Plates	*210*	*183*

In addition to changing some material properties, also the connections were tuned. The connection type between the midframe and stator was changed to frictional contact, with friction coefficient of 0.2. this was done to reduce the stiffness of the frame models. Also the bearing stiffnesses were tuned to validate the complete assembly. The updated parameters are presented in table 14.

Table 14. The updated bearing stiffnesses of the validated motor models.

	Parameter	***Original values***	***Updated Values***
EM1	*DE - Radial Stiffness*	*184 333*	*497 700*
	NDE - Radial Stiffness	*178 667*	*482 400*
	DE - Axial Stiffness	*1 782*	*1 782*
	NDE - Axial Stiffness	*1 990*	*1 990*
EM2	*DE - Radial Stiffness*	*99 933*	*999 333*
	NDE - Radial Stiffness	*143 000*	*1 430 000*
	DE - Axial Stiffness	*1 787*	*1 787*
	NDE - Axial Stiffness	*1 577*	*1 577*

The validation process was completed with these modifications to the parameters. Other materials and connections that were not mentioned in this chapter and the presented tables were not adjusted and remain same as presented in chapter 3.

6 DISCUSSION

The main goal of this thesis was to find the material properties of the rotor stack and validate the motor's FE models by comparing the numerical modal analysis to experimental. The modal analysis was done for stationary motors without any support. The acquired results and used parameters become non-valid as the motors are somehow supported or start to rotate. This is because the added supports affect the stiffness of the system, and the rotation adds new forces and affect the behavior of e.g. bearings.

By first studying the rotor and frame sub-assemblies, it was possible to minimize the number of variables at once. With original modal analysis, the rotor models gave 100% and 40% differences to the EMA. These values were acquired when the material stiffnesses were close to normal stiffness values of steel. The results of EMA show that the deformation of the rotor does not only occur in the ends of the shaft, but also from the middle where the rotor stack is (Figure 28a). This was not the case with the initial FEA models (Figure 28b).

During the model validation the material was changed into orthotropic material and the axial stiffness was reduced to 4 GPa for the smaller rotor stack and 2 GPa for the larger. With the updated material properties, the differences to the EMA were reduced to $< 2\%$. Now by inspecting the modals shapes of the rotor, one can see that the deformations occur also in the FE models (Figure 28c).

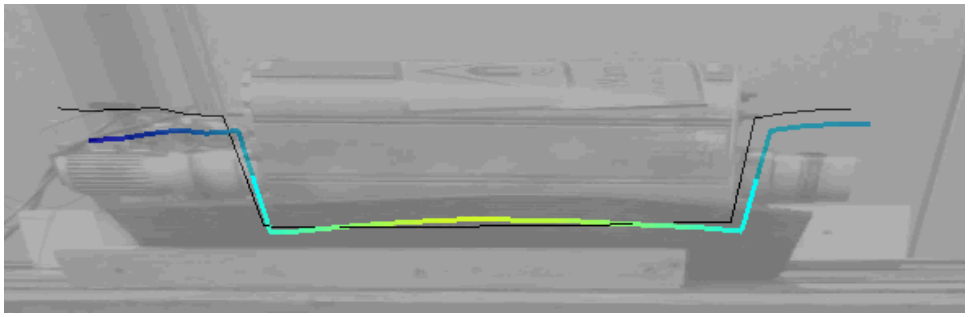

(a)

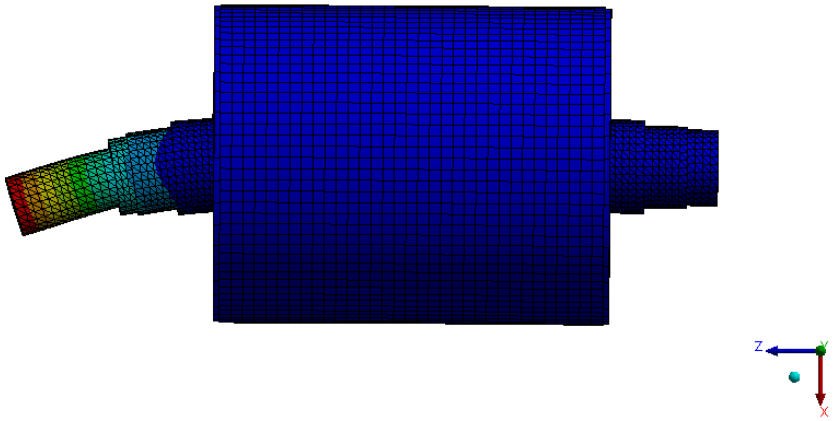

(b)

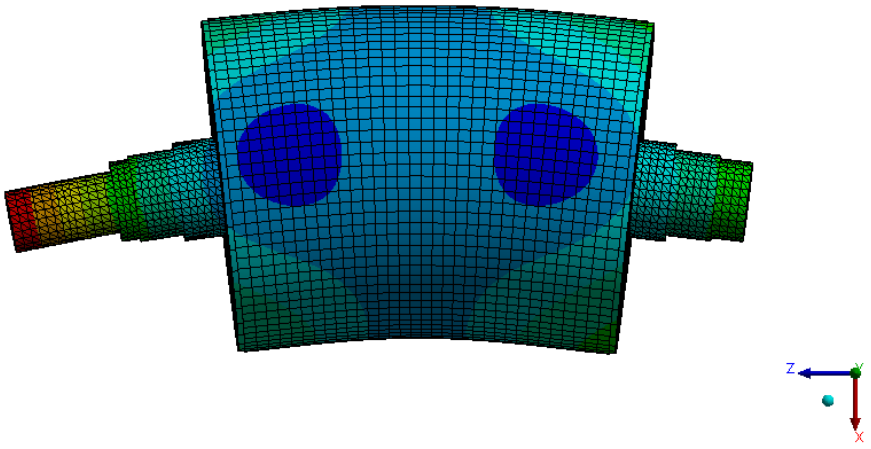

(c)

Figure 28. In the initial results of FEA (b), the deformations do not correspond the results of EMA (a). After validation process the deformations of FEA (c) are much similar to the EMA.

This, in validation viewpoint, is a good result but the new material stiffnesses are quite low for a metal structure, since elastic modulus of 2 – 4 GPa corresponds e.g. some polymers,

fiberboards and epoxy resins. This implies that the laminated rotor stack does not significantly stiffen the rotor.

However, it is still possible that e.g. the assumed bonded connection between the shaft and rotor stack is too stiff, or the design is behaving stiffer than intended. This is why, the stiffness of the stack may be lower than it really would be. It is possible that using the suggested branched model from literature would eliminate this problem.

The initial frame model of the smaller motor did not have as large differences to EMA as the rotors had in the beginning. By analyzing the smaller motor's mode shapes from FEA, it was possible to notice that especially modes related to the NDE plate of the motor were hard to find and had greatest differences to EMA. Also, the fact that the modes of DE were lower than NDE's, while in EMA the situation was another way around, showed that the results were not perfect. This could be because of the simplified models that were created for this study. The simplified design does not include all the indentations and asymmetrical features. This may cause some areas to have more or less material than the real system.

The model of the larger motor had a similar problem. The frame of the larger motor had over 100% differences to the EMA with modes relating to the middle frame of the motor. Since it seemed that the bonded connection between the stator and midframe was too stiff, the connection was changed to frictional. This did not improve the results enough and the material properties of the frame were modified. By decreasing the Young's modulus of the end plates' to 183 GPa and stator's and midframe's to 100 GPa the maximum difference between FEA and EMA was decreased to 7%.

However, Young's modulus of 100 GPa for a steel structure is low. It is possible that the model contains some errors caused by the model simplification and this stiffens the structure excessively. The frame of the larger motor also contains cooling pathways on the surface (Figure 29).

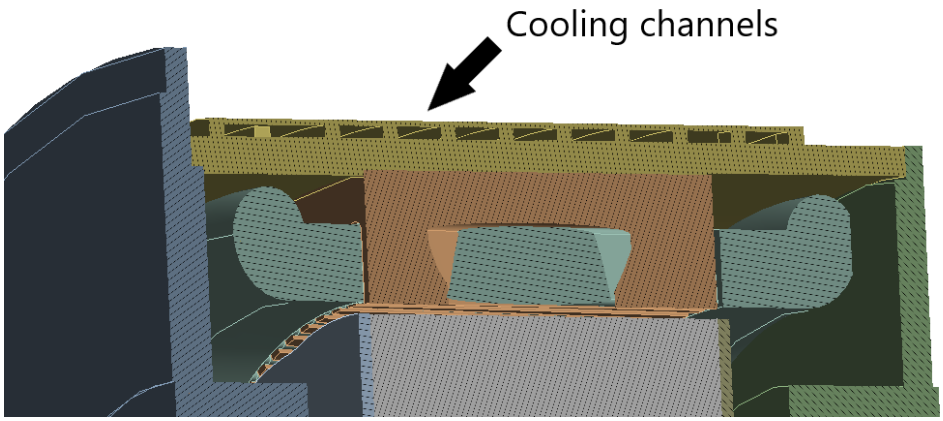

Figure 29. The surface of EM2's frame has pathways for cooling purposes.

It is possible that these have affected either the experimental measurements or the numerical modal analysis so that the results are corrupted.

By validating the two sub-assemblies first and then continuing to the validation of the whole model was a good principle. This way the number of variables at once was kept as low as possible. However, the validation of the whole assembly included two bearings with their own parameters. This created 4 – 6 variables to the validation process of the whole assembly. In this study the radial stiffnesses in *X* and *Y* direction were assumed as equal so the number of variables was four. Also, the errors of the subassemblies carried out to the main assembly, which might be the reason for some larger differences between the FEA and EMA.

During the validation process it was noticed that changing the bearing stiffnesses had little effect to the natural frequencies of the frame, but the natural frequencies of the rotor could be adjusted. However, unlike the literature suggested these stiffness values were increased and not decreased. Kastinen (2019) suggested that computationally estimated bearing stiffnesses can be significantly higher than the real values. In this study the stiffnesses of validated models were even ten times of the estimated values.

It is possible that the models used to determine the estimated bearing stiffnesses were too simple. For the models the rotor stack was modelled as a solid part of the shaft with equivalent diameter and the mass of the whole rotor was set as a point mass to the center of mass of the system. However, these values were meant to be changed during the validation

process, so the accuracy was not needed. The final values of the bearing stiffnesses are reasonable.

According to EMA, both motors have very low natural frequencies for the rotors. In the previous rotor models the first natural frequencies were found at 800 – 900 Hz, but here they are at 200 – 300 Hz. This can be caused by the supports that are added to the system, which in this case are the bearings. Adding stiff bearings to the system, can cause the rigid modes of the shaft to jump and create mode shapes for the lower frequencies as seen in Figure 30 (Kaneko, Kanki & Kawashita 2017, p. 145).

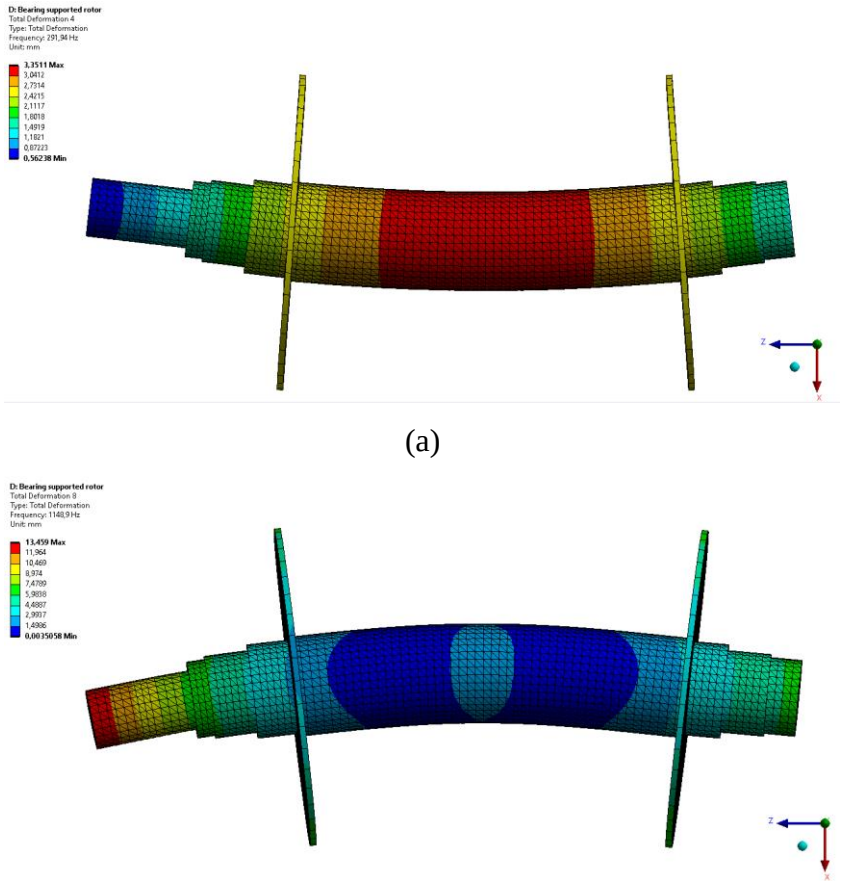

Figure 30. With stiff bearings, the rigid translation of the shaft transforms into mode (a), which is similar to the 1st bending mode (b).

The rigid translation of the shaft transforms into mode, which is similar to the 1st bending mode. Here the deformations occur in the middle of the shaft rather than in the ends. This mode is low frequency and could explain why the first bending modes of the rotors are found

at 200 – 300 Hz in the assembly models. However, it is not possible to confirm this since the mode shapes from the EMA at these frequencies are not available. The same applies to all of the modes related to the rotor shapes in the full assembly models.

6.1 Key findings and novelty

The main goal of this thesis was successfully reached: The models of the rotor stacks were validated. In addition, also the complete assemblies were validated. Several mode shapes were successfully used for the validation process and overall, the differences between FEA and EMA were small. Some discontinuities were noticed but the possible causes have also been discussed.

The main goal of this study was to find the material properties of the rotor stack. This goal was successfully met. According to this study the rotor stack does not significantly increase the stiffness of the rotor. The acquired Young's moduli of the laminated rotor stacks in this study were 4.2 GPa and 2.4 GPa.

During the modelling process, it was noticed that ignoring the copper windings from the stator would decrease the natural frequencies significantly. This observation agrees with the results of Čorović & Miljavec (2020). Another observation is made about how the bearing stiffnesses impact on the results. In this thesis, unlike suggested by Kastinen (2019), the used bearing stiffnesses were significantly higher than the ones acquired by computational methods.

6.2 Reliability, validity and objectivity

The main purpose of this study was to validate the created FE models. This was done by utilizing experimental modal analysis to the same motors that were analyzed in Ansys. By comparing the results from FEA to the ones in EMA, it was possible to complete the validation process. The measurements were performed by professionals to collect as good data as possible.

The reliability of the results was increased by performing the same process for two different motors. For example, similar mode shapes were recognized from both motors. Also similar results were achieved with the model validation. This suggests that the main principle of this

thesis seems to be working. By performing literature review, studying the previous studies and using that data also increased the reliability of this thesis but also proved the objectivity of this work.

6.3 Error- and sensitivity analysis

There are many possibilities for errors in these kinds of studies where multiple methods are used. The number of errors is minimized by using literature and doing comparisons during and after the research. Still some errors may occur, which are most visible when comparing the validated FEA models to EMA.

Overall, the errors are caused since the simplified systems do not fully match the real ones. Deleting holes and other smaller details from the system might cause the resulting design being too rigid. It is also possible that these models contain some input errors like wrong dimensions. The possibility for these errors is minimized with steps like mass validation. Big mass differences in the model versus real motor might imply that wrong parameters or dimensions are used. Mass validation could be easily utilized for all the main components separately to ensure correct dividing of the masses. However modal analysis and model validation for each main component separately would not be reasonable. This would possibly create a more accurate model, but also be applicable to only one motor. Doing as detailed validation process for multiple systems would be time consuming and unnecessary.

It is good to remember that wear and tear of the R&D motors can cause differences to when compared to the FEA of an ideal motor. According to Čorović and Miljavec (2020) for example worn permanent magnets of the rotor might cause changes to the natural frequencies or even introduce new ones. In the FE model the permanent magnets are not modelled, and their places are filled.

Another source of error can be from wrong parameter combinations. For example, the bearings had multiple variables for their stiffness values. This makes it difficult to find good results but can also mean that there can be possible combinations that are not correct. It is important to remember that these combinations are motor specific. However, the principle is usable to validate FE models of stationary and freely supported electric motors.

6.4 Utilization and future research

This study shows the steps of model validation and proves that it can be successful. This thesis also achieved the initial goal of determining the material properties of the rotor stack. This information can be important for both customer and designer viewpoints when looking at the lifetime and development of the systems.

This study also shows the downfalls, where too many unknowns can make the validation process difficult. To improve this thesis and for further development of this topic the following areas should be tackled:

- The assemblies used for the model validation were mass validated. However, the masses of individual components can be wrong and distort the mass distribution of the models. Therefore, all the components should be mass validated at the beginning of the process.
- Closer inspection of the midframe of the larger motor is needed. It needs to be confirmed if the cooling channels have distorted the results of EMA or are the FE models of this thesis designed poorly.
- Since the experimental modal analysis was performed for a motor which did not match the created models, the measurements of the complete motor should be redone. After this the model validation can be redone and results updated.
- In this thesis the material properties of the windings and stators were approximations from the literature that feature different motors. These values were improved during the model validation, but the true material properties should be studied.
- In this thesis the bearing stiffnesses were computationally estimated values, which were then improved by manual testing. The acquired stiffnesses were higher than the ones from computational estimations and this is the opposite conclusion to the study of Kastinen (2019). Since the results are conflicting with previous studies, the topic should be investigated and bearing stiffnesses possibly redetermined.
- The mode shapes of the supported rotor are unknown and there is not certain if the selected validation pairs are really a pair. This could be studied and confirmed by performing EMA to a supported rotor assembly, where the stiffness of the support matches the stiffness of the bearing and the end plates in FE models.

Tackling these areas would improve the validity of the FE models even more. In addition, this thesis concentrated on freely supported and stationary motors without considering the wear of the motors or the changes that happen when the motor is mounted or rotating. These certainly are interesting cases from the perspective of manufacturers and their customers, and the ultimate goal would be to use virtual models to tell the effect of the age, supports and rotating speed to the real system.

7 CONCLUSION

The goal of this study was to validate the finite element models of the laminated rotor of an electric machine. This was done by comparing numerical modal analysis to experimental measurements. During the validation process the natural frequencies of the finite element analysis are matched with the experimental measurements.

Literature review was utilized to familiarize to the previous studies on the subject and to generate a solid plan to follow during the study. The study was performed for two stationary and freely supported motors, which both contain the same main components. The assemblies were divided into two sub-assemblies per motor, where one sub-assembly contained the rotor of the motor and the other contained the frame. This was done to validate parts of the assembly first and then combining the final model with less unknowns. The main points of interest during the validation process were the material properties of the rotor stack and the bearing stiffnesses between the rotor and frame. The metal structure of the motor frame was regarded simple enough structure with no major unknowns.

For the finite element modelling an un-branched method was used where the Young's modulus of the material was the only unknown. Other unknowns in the models were the bearing stiffnesses of the full assembly and the material properties of the stators and copper windings. Mass validation was performed to match the mases of the assemblies to the real ones and improve the accuracy of the models.

A numerical modal analysis was generated for the finite element models and the results compared with the experimental modal analysis. During the validation process the finite element analysis was continuously compared to the experimental measurements while changing the unknown parameters. With this method it was possible to achieve close enough results between FEA and EMA.

According to this study the laminated rotor stack would not stiffen the rotor structure significantly. The orthotropic material used for the finite element models had an axial Young's modulus of 2 – 6 GPa, which corresponds to e.g. fiberboard or some polymers.

Other observation includes that the estimated bearing stiffnesses acquired with computational methods were low. After the validation process the updated models suggest that some areas of the used models are behaving too rigidly or there are errors caused in the measurements. Also, some uncertainties and unknown parameters still remain in the models. These in mind improvements for this thesis and topics for further studies are suggested.

REFERENCES

Abbey, T. 2015. Verification and Validation in Relation to FEA. [web document]. [Referred 14.5.2021]. Available: https://www.digitalengineering247.com/article/verification-vs-validation/

Alta solutions. 2012. AS-1220 Automated impact hammer. [www- data sheet]. [Referred 13.5.2021]. Available: https://cdn.thomasnet.com/ccp/10076081/66771.pdf

Breunig, J. 2017. Bolted Connections Are Not as Simple As They Seem. [web document]. [Referred 2.6.2021]. Available: https://www.xceed-eng.com/bolted-connections/

Budynas, R. & Nisbett, J. 2011. Shigley's Mechanical Engineering Design. Ninth Edition.

Cavalini, A., Lobato, F., Koroishi, E. & Steffen, V. 2015. Model updating of a rotating machine using the self-adaptive differential evolution algorithm. In: Inverse Problems in Science and Engineering. Volume 24, Issue 3, Pp. 504 – 523.

Čepon, G., Pirnat, M. & Boltežar, M. 2012. An experimental and numerical identification of laminated structure dynamics. In: Proceedings of ISMA2012-USD2012. Pp. 3153 – 3166.

Čorović, S. & Miljavec, D. 2020. Modal Analysis and Rotor-Dynamics of and Interior Permanent Magnet Syncronous Motor: An Experimental and Theoretical Study. In: Applied Sciences. Volume 10, Issue 17.

Danfoss, 2021. Danfoss Editron. [Danfoss webpage]. [Referred 21.3.2021]. Available: https://www.danfoss.com/en/about-danfoss/our-businesses/power-solutions/danfoss-editron/

Devesoft. 2021. Modal testing. [web document]. [Referred 20.5.2021]. Available: https://dewesoft.com/daq/what-is-modal-analysis#modal-testing

Garvey, S., Penny, J., Friswell, M. & Lees, A. 2004. The stiffening effect of laminated rotor cores on flexible-rotor electrical machines. In: Vibrations in Rotating Machinery. Volume 1000, Issue 1, Pp. 193 – 202.

Hanejko, F. 2020. Induction VS Permanent Magnet Motor Efficiency | Auto Electrification. [web document]. [Refered 21.3.2021]. Available: https://www.horizontechnology.biz/blog/induction-vs-permanent-magnet-motor-efficiency-auto-electrification

Kaneko, Y., Kanki, H. & Kawashita, R. 2017. Steam turbine rotor design and rotor dynamics analysis. In: Advance in Steam Turbines for Modern Power Plants. 2017. Pp. 127 – 152.

Kastinen, M. 2019. Rolling-element bearing stiffness estimation from relative shaft displacement.

Matyja, T. 2015. Simplified method of modelling the bearing supports in rotating systems. In: Journal of Vibroengineering. Volume 18, Issue 1, Pp. 93 – 102.

Mechanicalc 2021. Bolted Joint Analysis. [web document]. [Referred 2.6.2021]. Available: https://mechanicalc.com/reference/bolted-joint-analysis

Mottershead, J. & Friswell, M. 1993. Model updating in structural dynamics: Survey. In: Journal of Sound and Vibration. 1993. Volume 167, Issue 2, Pp. 347 – 375.

Murphy, J. 2012. What's the difference Between AC Induction, Permanent Magnet, and Servomotor Technologies? [web document]. [Referred 21.3.2020]. Available: https://www.machinedesign.com/motors-drives/article/21831709/whats-the-difference-between-ac-induction-permanent-magnet-and-servomotor-technologies

Nutakor, C. 2014. Modal testing and numerical modelling of the dynamic properties of layered sheet-steel structure.

Polytec 2012. Basic Principle of Laser-Doppler Vibrometry. [Youtube video]. [Referred 13.5.2021]. Available: https://www.youtube.com/watch?v=o0qkmG_S4QY&t=67s

Polytec 2021a. Laser Doppler vibrometry. [Polytec webpage]. [Referred 13.5.2021]. Available: https://www.polytec.com/eu/vibrometry/technology/laser-doppler-vibrometry

Polytec 2021b. PSV-500 Scanning Vibrometer. [Polytec webpage]. [Referred 13.5.2021]. Available: https://www.polytec.com/eu/vibrometry/products/full-field-vibrometers/psv-500-scanning-vibrometer

Santos, H., Luersen, M. & Bavastri, C. 2013. Experimental evaluation of numerical models to represent the stiffness of laminated rotor cores in electrical machines. In: Journal of Engineering Science and Technology. Volume 8, Issue 4, Pp. 457 – 471.

Skotny, Ł. 2019. What are the types of Elements used in FEA? [web document]. [Referred 12.5.2021]. Available: https://enterfea.com/what-are-the-types-of-elements-used-in-fea/

Tufoi, M., Gillich, G., Praisach, Z., Ntakpe, J. & Hatiegan, C. 2014. An Analysis of the Dynamic Behaviour of Circular Plates from a Damage Detection Perspective. In: Romanian Journal of Acoustics and Vibration. 2014. Volume 11, Issue 1, Pp. 41 – 46.

Veikos, N. 2016. Verifying Your Finite Element Analysis Results. [web document]. [Referred 14.5.2021]. Available: https://www.engineering.com/story/verifying-your-finite-element-analysis-results

What-when-how.com 2021. FEM for 3D Solids (Finite element Method) Part 1. [web document]. [Referred 12.5.2021]. Available: http://what-when-how.com/the-finite-element-method/fem-for-3d-solids-finite-element-method-part-1/

EMA natural frequencies and mesh settings

In this appendix the results of the experimental measurements are listed and the meshes, which were used to acquire them.

The first experimental measurements were done for EM2. The acquired frequencies are listed in table below

The natural frequencies of EM2 from experimental measurements

EM2 - EMA Results					
Rotor		Frame		Assembly	
Freq [Hz]	Part	Freq [Hz]	Part	Freq [Hz]	Part
810		415	DE	359	Rotor
866		555	DE	1020	Rotor
1580		708	DE	1120	Rotor
1820		818	DE	650	DE
1960		1030	DE	1020	DE
		1730	DE	1110	DE
		2090	DE	1250	DE
		2730	DE	1540	DE
		415	NDE	2700	DE
		708	NDE	2740	DE
		1030	NDE	413	NDE
		1750	NDE	515	NDE
		2080	NDE	678	NDE
		2700	NDE	1120	NDE
		420	Side	1190	NDE
		1030	Side	1990	NDE
		1750	Side	2740	NDE
		2500	Side	3070	NDE
				128	Side
				400	Side
				520	Side
				680	Side
				935	Side
				1120	Side
				1250	Side
				1400	Side

The results of the experimental measurements for EM1 are listed below.

The natural frequencies of EM1 from experimental measurements

EM1 - EMA Results					
Rotor		Frame		Assembly	
Freq [Hz]	Part	Freq [Hz]	Part	Freq [Hz]	Part
968		616	Side	203	Side
1811		693	NDE	292	Rotor
		798	DE	294	NDE
		1000	NDE	300	Side
		1041	Side	339	DE
		1043	DE	460	NDE
		1144	Side	623	Side
		1273	DE	726	DE
		1273	NDE	760	NDE
		1664	NDE	1160	Rotor
		1970	NDE	1330	DE
		2023	Side	1670	NDE
		2263	NDE	1700	DE
		2294	DE	1720	Rotor
		2636	Side	1780	Side
		2883	DE	2230	Side
		2923	Side	2610	NDE
		2975	NDE	2820	DE
		3143	DE	2850	NDE
		3330	NDE	3010	DE
		3705	NDE		

In following pictures, the meshes used in experimental measurements are presented.

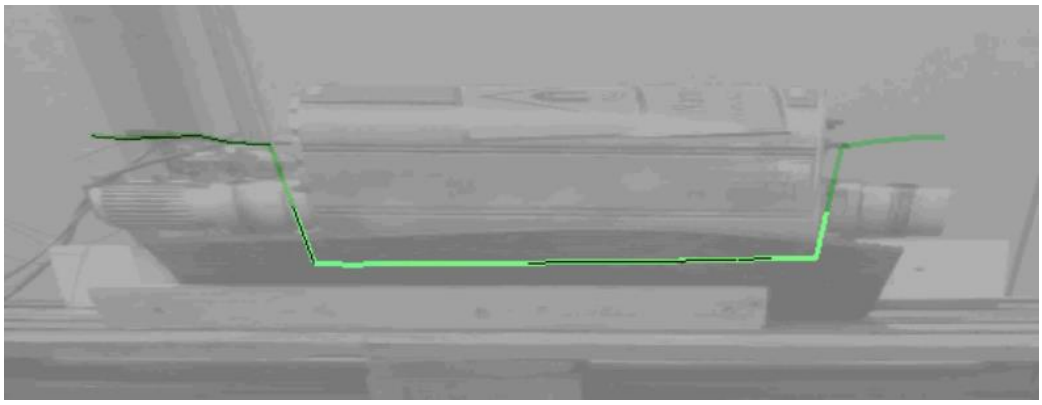

Mesh of the EM1 rotor

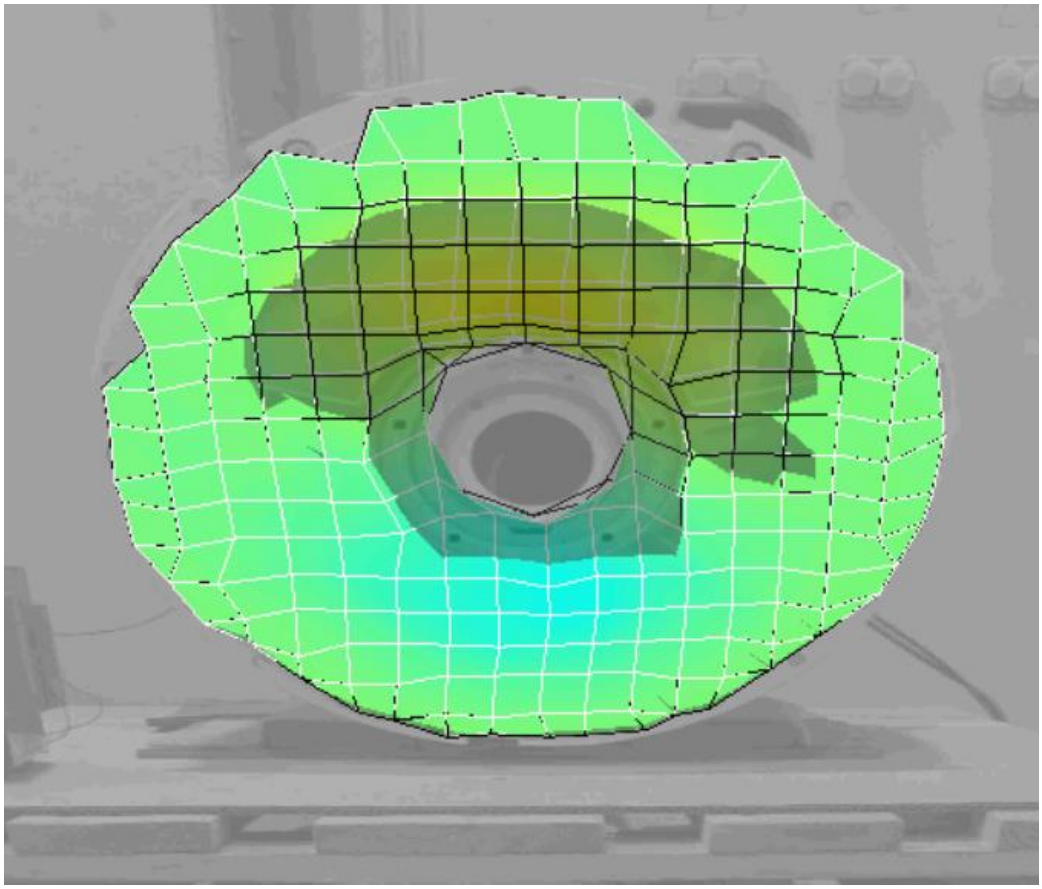

Mesh of the EM1 DE plate

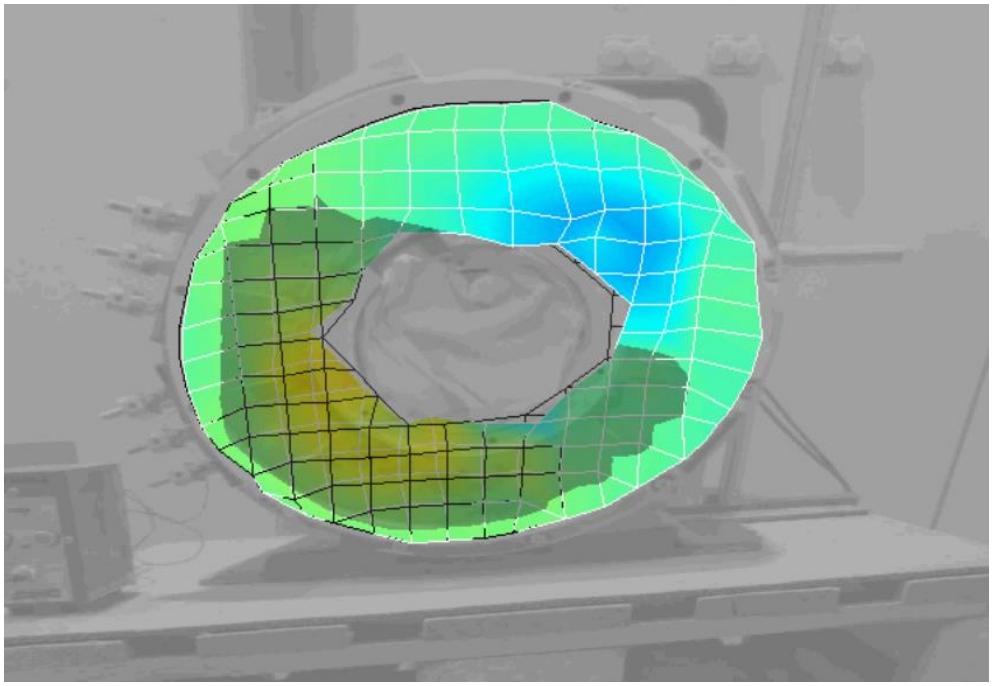

Mesh of the EM1 NDE plate

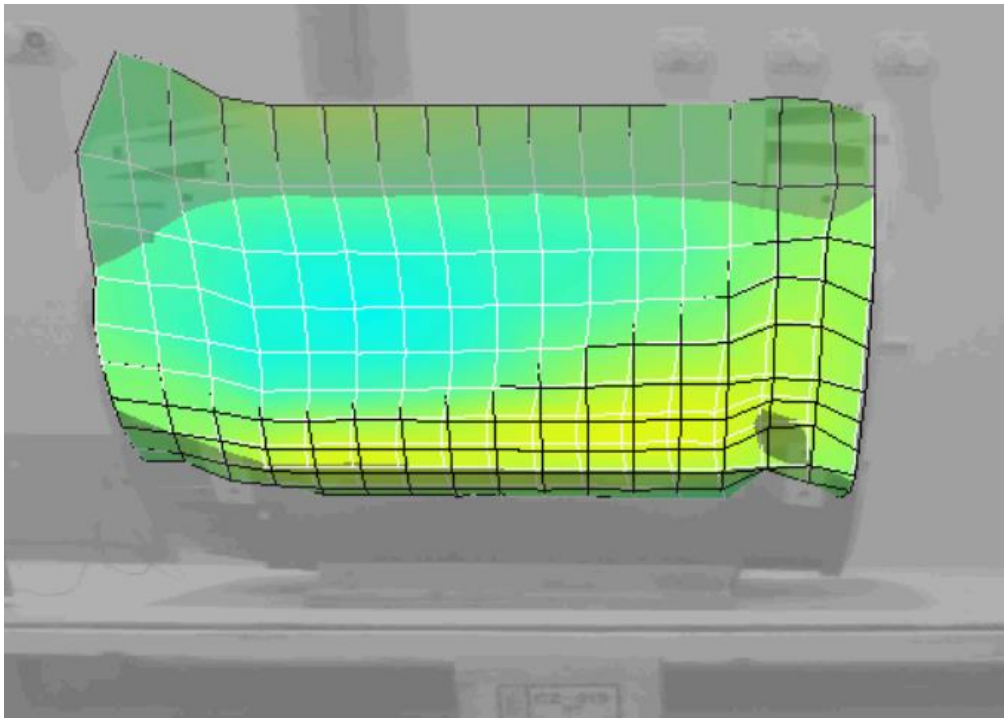

Mesh of the EM1 midframe

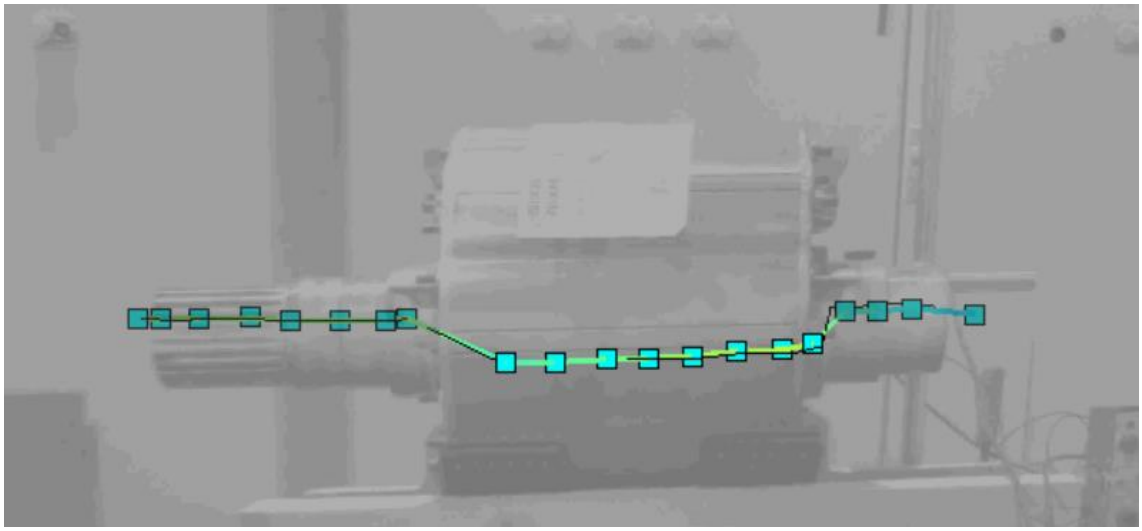

Mesh of the EM2 Rotor

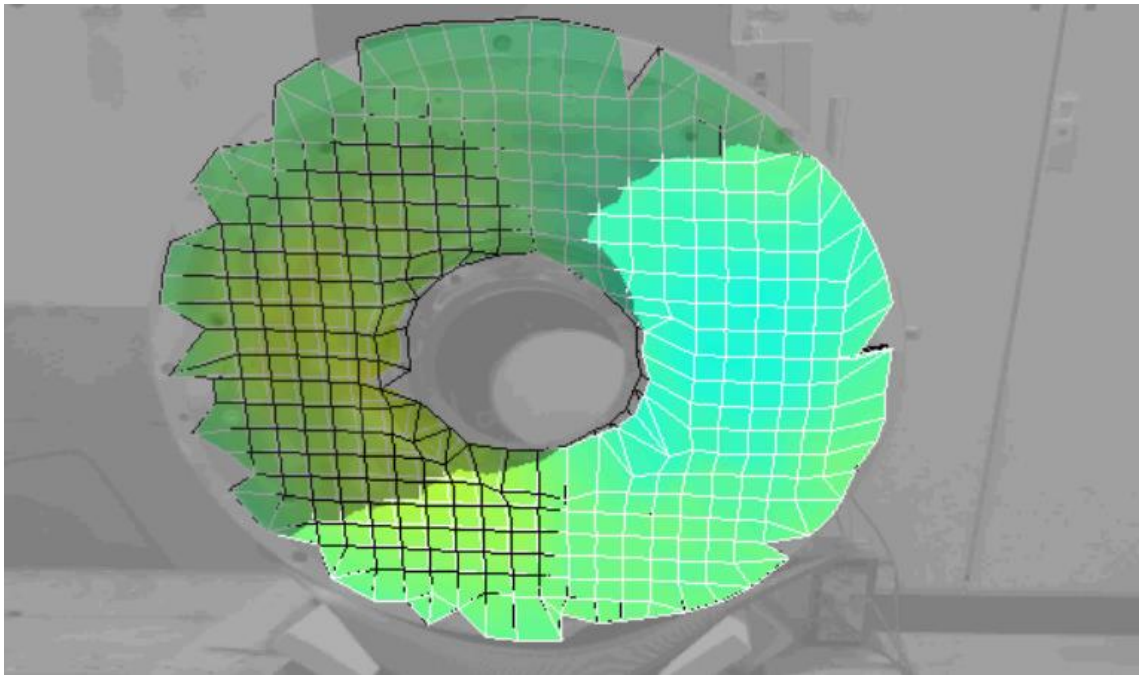

Mesh of the EM2 DE plate

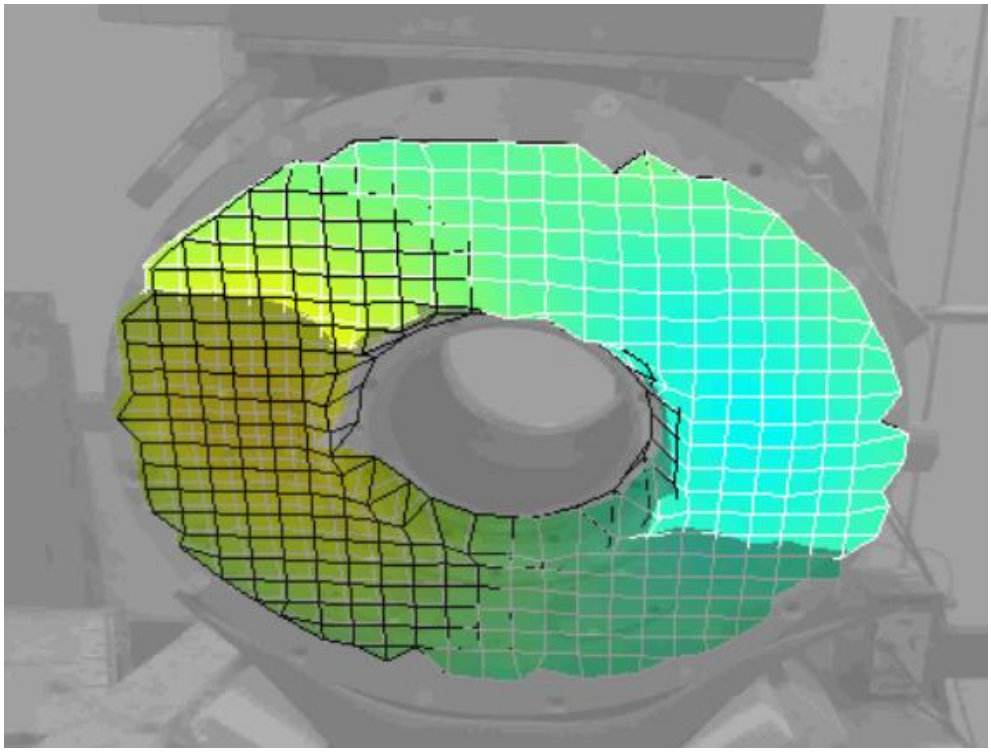

Mesh of the EM2 NDE plate

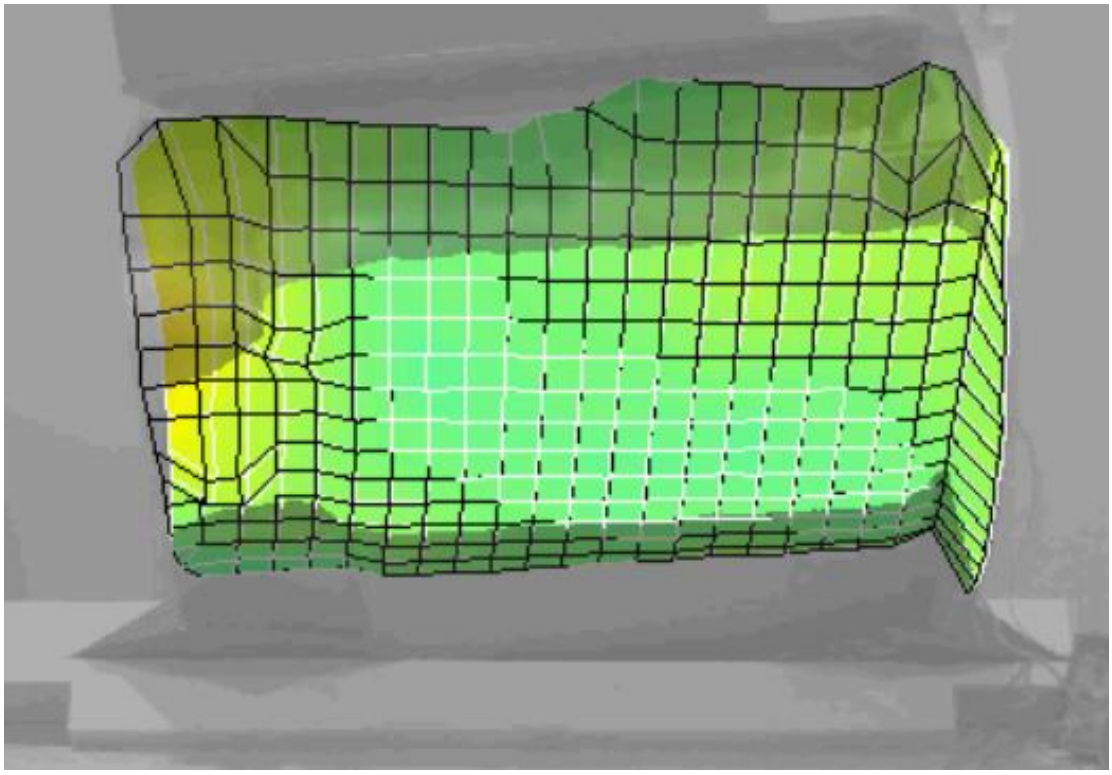

Mesh of the EM2 midframe